© 2020. Published by The Company of Biologists Ltd | Journal of Experimental Biology (2020) 223, jeb218032. doi:10.1242/jeb.218032

RESEARCH ARTICLE

Coding of odour and space in the hemimetabolous insect *Periplaneta americana*

Marco Paoli[1,*], Hiroshi Nishino[2], Einat Couzin-Fuchs[1] and C. Giovanni Galizia[1,*]

ABSTRACT

The general architecture of the olfactory system is highly conserved from insects to humans, but neuroanatomical and physiological differences can be observed across species. The American cockroach, inhabiting dark shelters with a rather stable olfactory landscape, is equipped with long antennae used for sampling the surrounding air-space for orientation and navigation. The antennae's exceptional length provides a wide spatial working range for odour detection; however, it is still largely unknown whether and how this is also used for mapping the structure of the olfactory environment. By selectively labelling antennal lobe projection neurons with a calcium-sensitive dye, we investigated the logic of olfactory coding in this hemimetabolous insect. We show that odour responses are stimulus specific and concentration dependent, and that structurally related odorants evoke physiologically similar responses. By using spatially confined stimuli, we show that proximal stimulations induce stronger and faster responses than distal ones. Spatially confined stimuli of the female pheromone periplanone B activate a subregion of the male macroglomerulus. Thus, we report that the combinatorial logic of odour coding deduced from holometabolous insects applies also to this hemimetabolous species. Furthermore, a fast decrease in sensitivity along the antenna, not supported by a proportionate decrease in sensillar density, suggests a neural architecture that strongly emphasizes neuronal inputs from the proximal portion of the antenna.

KEY WORDS: Olfaction, Odour coding, Calcium imaging, Antennal lobe, Insects, Cockroach

INTRODUCTION

The olfactory system is highly conserved across species (Galizia and Rössler, 2010; Hildebrand and Shepherd, 1997; Kay and Stopfer, 2006). Nevertheless, differences in the neural architecture and physiology can be observed. The American cockroach *Periplaneta americana* is a gregarious animal, often living in dark shelters with a rather stable olfactory landscape. It is equipped with exceptionally long antennae (up to 5 cm, often exceeding its body length) that actively sample the surrounding air-space for orientation and navigation. Long antennae allow a wide working range for odour detection. However, it is still largely unknown whether and how this could be used for mapping the spatial structure of the olfactory surroundings. Insects rely on bilateral comparison of antennal inputs and on their temporal integration for perceiving the distribution of odorants in space (Borst and Heisenberg, 1982; Gomez-Marin, 2010; Takasaki et al., 2012). Nonetheless, it has recently been suggested that odour source localization in cockroaches may rely more on the overall antennal length than on bilateral inputs (Lockey and Willis, 2015). Cockroach antennae are covered in sensilla, cuticular structures of different size and shape, together hosting approximately 220,000 olfactory sensory neurons (OSNs) (Sass, 1983; Schaller, 1978). Olfactory neurons originating in different locations along the antenna converge into the antennal nerve, and descend towards the antennal lobe (AL), the first odour-processing centre, which is structured into ∼205 anatomical and functional units, named glomeruli (Watanabe et al., 2010). Each glomerulus receives inputs from on average 1000 OSNs originating in different antennal segments (annuli), probably all expressing the same olfactory receptor gene. The male cockroach possesses an additional ∼36,000 OSNs for the detection of the minor and major components of the female sex pheromone, periplanone A and B, respectively (Sass, 1983; Schaller, 1978; Watanabe et al., 2012). Their axons innervate two exceptionally large glomeruli, which form the macroglomerular complex (Schaller, 1978; Watanabe et al., 2012). Glomeruli are interconnected by a dense network of local interneurons (Fusca et al., 2013; Husch et al., 2009), and processed olfactory information is relayed to higher order brain centres by uniglomerular (uPNs) and multiglomerular projection neurons (mPNs) (Malun et al., 1993). uPNs extend their dendritic arborization in a single glomerulus, thus receiving direct input from only one OSN type. Two subgroups of uPNs innervate distinct glomerular populations, their cell bodies clustering in two distinct groups in the antero-dorsal side of the AL (Strausfeld and Li, 1999; Watanabe et al., 2017). In the American cockroach, each ordinary glomerulus is innervated by only one uPN, whereas the macroglomerulus (MG) is innervated by multiple uPNs with a highly stereotyped topology (Galizia, 2018; Nishino et al., 2018). Two main projection neuron (PN) axon bundles exit from the medio-dorsal side of the AL (note that all orientations here provided are in body axis system), and relay odour-related information to the protocerebrum. A first thick and more medial root splits in three distinct AL tracts [ALTs (Ito et al., 2014), previously termed antenno-cerebral tracts, ACTs (Malun et al., 1993)]: ALT-I (also inner-ALT), ALT-II and ALT-III. They comprise the uPN axons, and innervate both the mushroom body (MB) calices and the lateral protocerebrum (LP). Posterior to the first root, a second bundle of axons exits the AL forming the ALT-IV and the outer-ALT. These lateral tracts collect the axons from mPNs, and innervate almost exclusively the LP (Malun et al., 1993).

Cockroaches are hemimetabolous insects. Hence, the basic structures of the brain are established during embryogenesis, and gradually increase in volume during multiple post-embryonic moults. At each moult, new antennal segments are added

[1]Department of Neuroscience, University of Konstanz, 78457 Konstanz, Germany. [2]Research Institute for Electronic Science, Hokkaido University, Sapporo 060-0812, Japan.

*Authors for correspondence (giovanni.galizia@uni-konstanz.de; marco.paoli@uni-konstanz.de)

M.P., 0000-0001-5672-1403; E.C.F., 0000-0001-5269-345X; C.G.G., 0000-0001-8292-6031

Received 4 November 2019; Accepted 6 January 2020

Journal of Experimental Biology (2020) 223, jeb218032. doi:10.1242/jeb.218032

proximally to the head, together with new OSNs (Schafer and Sanchez, 1973; Watanabe et al., 2018). As shown for the MG (Nishino et al., 2018) and suggested for common glomeruli (Nishino and Mizunami, 2007), OSN axons descend along the antennal nerve and terminate onto the AL glomeruli, forming segment (and thus age)-specific layers of OSN terminals from the core to the cortex of each glomerulus, producing an antennotopic innervation (Nishino et al., 2018). In this respect, they differ from holometabolous insects, which develop the complete glomerular organization during a single metamorphic event, and where the innervation topology does not reflect a sequence of post-embryonic moults (although it may still be antennotopic). In all insects, AL output neurons develop during embryogenesis. However, whereas the holometabolous insects studied so far are generally equipped with multiple uPNs per glomerulus [fruit fly: 50 glomeruli and 150–200 uPNs (Grabe et al., 2015; Stocker et al., 1997); moth: 60 glomeruli and 740 uPNs (Homberg et al., 1988); honeybee: 165 glomeruli and 800 uPNs (Brandt et al., 2005; Galizia et al., 1999b; Rybak et al., 2010)], in the American cockroach, each glomerulus is innervated by a single uPN (Ernst and Boeckh, 1983). Such an architectural difference should have an impact on the AL network coding properties, and might indicate species-specific adaptations to the environment, and distinct evolutionary strategies to efficiently encode olfactory inputs.

Recently, Nishino et al. (2018) showed an antennotopic distribution of pheromone-sensitive ORNs and their uPNs, which allows the spatial encoding of pheromone plumes along a single antenna (Nishino et al., 2018). Such an antennotopic organization could provide the means for encoding spatial information of complex olfactory environments. This becomes particularly relevant in dense dark shelters, where insects are required to rely heavily on smell. In such conditions, the ability to assess the spatial structure of a stimulus could provide pivotal information for odour-source localization. In addition, spatial separation can also aid in differentiating between homogeneous and heterogeneous mixtures, because in the latter, plumes have pockets of different odour quality, and thus can be used to identify different odorant sources (Nowotny et al., 2013; Stierle et al., 2013).

Here, by selectively labelling AL uPNs, we studied how olfactory stimuli of different nature and concentration are encoded within the AL of a hemimetabolous insect. We selected a pool of single-molecule odorants with different degrees of similarity that have been shown to be perceived and discriminated by the American cockroach (Arican et al., 2019; Boeckh and Ernst, 1987; Gehret et al., 2001; Sakura and Mizunami, 2001; Sakura et al., 2002) to probe how structural relatedness is encoded in the glomerular space. We also included peppermint oil among the chosen odorants, because of its negative valence (Gehret et al., 2001; Matsumoto et al., 2012; Sakura and Mizunami, 2001), and two natural odorants, isoamyl acetate and butanol, respectively found in bananas and fermenting fruits. Furthermore, we extended the investigation of spatial coding to also include non-pheromone odour groups. We applied spatially confined stimuli to assess stimulus sensitivity along the antenna, and investigated how responses of AL output neurons (i.e. uPNs) change according to the stimulus nature, concentration and location.

MATERIALS AND METHODS

Animal preparation

Adult males of the American cockroach, *Periplaneta americana* (Linnaeus 1758), were kept on a 12 h/12 h light/dark cycle at 24°C and 65% humidity in the animal facility of the University of Konstanz (Germany). Male cockroaches were collected and briefly anaesthetized with CO_2 to facilitate handling. For neuroanatomy, a glass capillary coated with the fluorescent tracer Alexa Fluor 568 conjugated with 10 kDa dextran (all Alexa Fluor dyes were from Thermo Fisher Scientific, Waltham, MA, USA) was injected into the AL. For uPN/mPN double-labelling, 10 kDa dextran-conjugated Alexa Fluor 488 and Alexa Fluor 647 were injected medio-ventrally to the medial calix of the MB and medio-ventrally to the LP, respectively. Dye-injected specimens were incubated in a humid chamber at 4°C for 24 h. The following day, brains were dissected, fixed in 4% paraformaldehyde (PFA) in phosphate-buffered saline (PBS) for 3 h at 4°C, dehydrated in ascending concentrations of ethanol, cleared in xylene, and mounted in DPX mounting medium (Sigma-Aldrich, St Louis, MO, USA). Animal preparation for PN calcium imaging was adapted from a protocol previously established in honeybees (Paoli et al., 2017; Sachse and Galizia, 2002). On the first day, male cockroaches were anaesthetized and placed in a custom-built holder. The head was restrained with soft dental wax and a small window was opened in the head cuticle to expose the injection site. For uPN labelling, the tip of a glass capillary coated with 10 kDa dextran-conjugated Fura-2 (Thermo Fisher Scientific) was injected ventro-medially into the medial MB calix, where ALT-I/II (Malun et al., 1993) travel along the MB. For mPN labelling, the injection was directed to the ventro-medial side of the LP, where the outer-ALT formed by mPN axons enters the LP (Malun et al., 1993). All animals used in this study were labelled on the right side of the brain only. After dye injection, the head capsule was closed to prevent brain desiccation. The following day, the AL was exposed to allow optical access, and the brain was covered in transparent two-component silicon (Kwik-Sil, WPI, Sarasota, FL, USA). In this procedure, the degree of labelling depends on the precision of the injection site and on the amount of dye loaded on the glass capillary. Hence, a variable level of PN labelling may result. To investigate the topology of OSN axon terminals, selective degeneration of OSNs was induced by amputating distal antennal segments. The flagellum of a briefly anaesthetized cockroach was left intact or cut at different proximal–distal sections (25%, 50%, 75% or 100% amputation). Cockroaches were then kept in a dark cage with food and water supplied *ad libitum* for a 7 day recovery period. During this time, all OSNs originating in the amputated part of the antenna degenerated, and their axon terminals disappeared (Distler and Boeckh, 1997; Nishino et al., 2018). After a week, the antennal nerve was cut at the scape and placed into a glass capillary loaded with an aqueous solution of 10 kDa dextran-conjugated Alexa Fluor 555. In parallel, uPNs were labelled as described above with 10 kDa dextran-conjugated Alexa Fluor 488. PN labelling was used as reference to quantify glomerular volume even after partial degeneration of the OSN terminals. Dye-injected specimens were incubated in a humid chamber at 4°C for 24 h, after which the brain was dissected, and processed for confocal microscopic observation. Thirty-seven specimens were prepared for this analysis.

Neuroanatomy

Whole-brain sections (Fig. 1A; Movie 1) were acquired with a LSM 5 PASCAL laser scanning confocal microscope (Carl Zeiss, Jena, Germany) at a resolution of 1.16 µm pixel^{-1} (x, y) and 2 µm z-intervals using a 10× dry objective (Zeiss Plan-Apochromat 10×/0.45). AL optical sections with uPNs/mPNs labelling (Fig. 1C) were acquired with an LSM 510 laser scanning confocal microscope (Carl Zeiss) at a resolution of 0.77 µm pixel^{-1} (x, y) and 3 µm z-intervals using a 10× water-immersion objective (Zeiss

Journal of Experimental Biology (2020) 223, jeb218032. doi:10.1242/jeb.218032

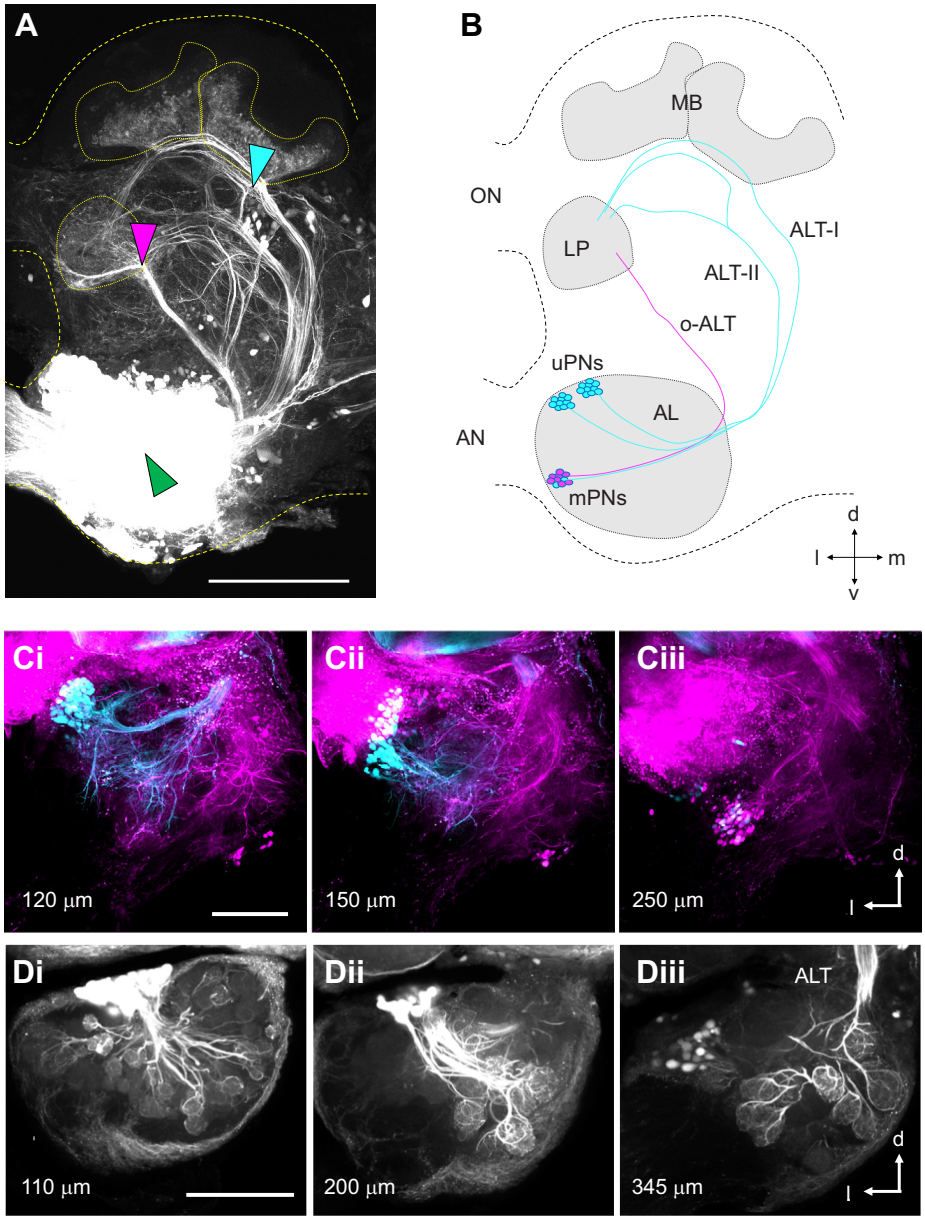

Fig. 1. Antennal lobe projection neuron labelling. (A) Antennal lobe (AL) injection (green arrowhead) reveals the main projection neuron (PN) tracts. Local injection ventro-medial to the medial mushroom body (MB) calix (cyan arrowhead) labels uniglomerular projection neurons (uPNs); injection ventral to the lateral protocerebrum (LP; magenta arrowhead) labels multiglomerular projection neurons (mPNs). (B) Drawing of the main PN tracts. ALT, antennal lobe tract (o, outer); AN, antennal nerve; MB, mushroom body calyces; ON, optic lobe nerve. (C) Double labelling for uPNs (cyan) and mPNs (magenta), at different focal depths within the AL. Note the distinct cell clusters for both populations. (D) uPN labelling at different focal depths within the AL. Note the clear staining of olfactory glomeruli. Acquisition depth along the AL antero-posterior axis is indicated in each panel of C and D. l, lateral; d, dorsal. Scale bars: 200 µm.

C-Apochromat 10×/0.45w); AL optical sections with uPNs labelling (Fig. 1D) were acquired at a resolution of 0.54 µm pixel^{-1} (x, y) and 1 µm z-intervals using a 20× water-immersion objective (Zeiss W-Plan-Apochromat 20×/1.0); AL optical sections for glomerular volume reconstruction (Fig. 2) were acquired at a resolution of 0.38 µm pixel^{-1} (x, y) and 3 µm z-intervals using a 20× water-immersion objective (Zeiss W-Plan-Apochromat 20×/1.0). ImageJ was used for image processing.

Calcium imaging

Calcium imaging of the MG (Fig. 3) was performed with an LSM 510 laser scanning microscope equipped with a Ti:sapphire two-photon laser (Chameleon Ultra, Coherent, CA, USA). The calcium-sensitive dye Fura-2 was excited with 750 nm pulses and emitted light was filtered through a 650 nm short-pass filter. The area corresponding to a central section of the MG was scanned at a 5 Hz frequency and with 2 µm pixel^{-1} (x, y) spatial resolution.

Calcium imaging analysis of AL PNs was performed with a wide-field fluorescence microscope (BX51WI, Olympus, Tokyo, Japan) equipped with a 10× water immersion objective (Olympus UM Plan FI 10×/0.30w). Images were acquired with a SensiCam CCD camera (PCO AG, Kelheim, Germany) with a 4×4 binning configuration resulting in 120×160 pixel size images (corresponding to 450×600 µm, with a pixel size of 3.75×3.75 µm). Recordings were performed at 5 Hz (for odour response maps; Fig. 4) or at 25 Hz (for measuring responses to localized stimuli; Fig. 5) using a TILLvisION acquisition system (TILL Photonics, Graefelfing, Germany). An LED system equipped with a 340 and a 385 nm LED (Omicron-Laserage Laserprodukte GmbH, Rodgau-Dudenhofen, Germany) was employed as a light source, which was directed onto the cockroach brain via a 410 nm short-pass filter and a 410 nm dichroic mirror. Emitted light was filtered through a 440 nm long-pass filter. Videos were exported and processed in Matlab (MathWorks Inc., Natick, MA, USA).

Odorant preparation

Odorants used were 1-butanol (CAS 71-36-3, cat. no. 19422-5ML), 1-pentanol (CAS 71-41-0, cat. no. 77597-1ML-F), 1-hexanol

Journal of Experimental Biology (2020) 223, jeb218032. doi:10.1242/jeb.218032

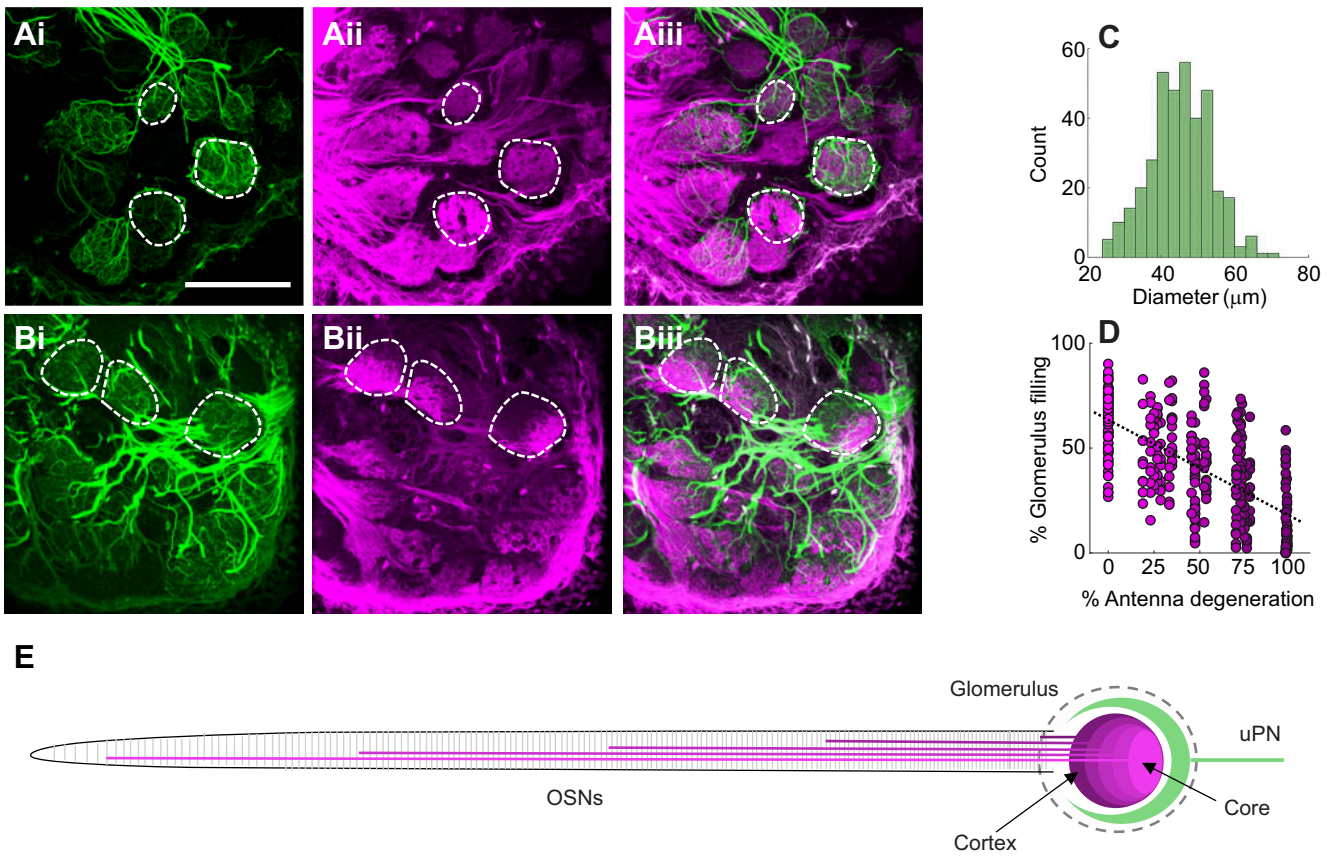

Fig. 2. Selective degeneration of olfactory sensory neurons reveals an antennotopic innervation pattern. (A,B) Optical section through an AL labelled for olfactory sensory neurons (OSNs; magenta) and for uPNs (green). In A, the antenna was left intact, whereas in B, 50% of the antenna was amputated before OSN tracing. Three representative glomeruli are circled. Scale bar: 200 µm. (C) Quantification of glomerular diameter (mean±s.d. 45±8 µm, *n*=369 glomeruli from 37 ALs). (D) Quantification of OSN glomerulus filling upon selective antennal nerve degeneration. Increasing the portion of degenerated antennal nerve induced progressive loss of innervation (linear regression analysis, R^2=0.43). (E) Schematic diagram of glomerular innervation topology based on OSN origin along the antenna according to our results and previous reports: proximal OSNs innervate the cortex and distal ones innervate the core of a glomerulus (Nishino and Mizunami, 2007; Nishino et al., 2018).

(CAS 111-27-3, cat. no. 73117-1ML-F), 1-heptanol (CAS 111-70-6, cat. no. 72954-1ML-F), 1-octanol (CAS 111-87-5, cat. no. 95446-5ML-F), 1-nonanol (CAS 143-08-8, cat. no. W278904-SAMPLE-K), 1-decanol (CAS 112-30-1, cat. no. W236500-SAMPLE-K), linalool (racemic, CAS 78-70-6, cat. no. L2602-100G), isoamyl acetate (CAS 193-12-2, cat. no. 79857-5ML) and peppermint oil (CAS 8006-90-4, cat. no. 77411-25 ml). All odorants were purchased from Sigma-Aldrich (St Louis, MO, USA) in the highest purity available. Odorants were used either pure or diluted in mineral oil (CAS 8042-47-5, cat. no. 124020010, Acros Organics, Thermo Fisher Scientific). Dilutions were prepared in 5 ml (for experiments with the PAL autosampler) or in 1 ml mineral oil (for experiments with spatially localized stimulation performed with the fast olfactometer) in 20 ml glass vials, covered with nitrogen (Sauerstoffwerk Friedrichshafen GmbH, Friedrichshafen, Germany) to prevent oxidation, and sealed with Teflon septum (Axel Semrau GmbH, Sprockhövel, Germany). Synthetic periplanone B (Kuwahara and Mori, 1990) was provided by Prof. Mark Willis to H.N. (Case Western Reserve University) diluted in hexane (CAS 110-54-3).

Odorant delivery

An automatic multi-sampler for gas chromatography (Combi PAL, CTC Analytics AG, Zwingen, Switzerland) was adapted for olfactory stimulation. Two 1 ml odour pulses were injected at 4 and 12 s with an injection speed of 1 ml s^{-1} into a continuous flow of 1 ml s^{-1} purified air. The stimulus was directed towards the antenna via a Teflon tube (inner diameter, 0.87 mm; length, 40 cm), and the antenna was inserted into the terminal portion of the tube to ensure similar stimulation conditions across animals. The first stimulus reached the antenna with ∼800 ms delay due to sampler path length and air flow. Hence, first stimulus onset was determined as 4.8 s. An inter-trial interval of 2 min was retained between odorants, during which the syringe was flushed with clean air. For each animal, the response to mineral oil was tested as a negative control. At the end of a stimulation cycle, the response to the first odorant was tested once again to assess the stability of odour responsiveness. After each set of odorants, the syringe was washed with *n*-pentane (Merk KgaA, Darmstadt, Germany), heated to 44°C and flushed with clean air. Each stimulation (i.e. stimulus preparation, delivery, syringe flushing, etc.) required ∼3 min. Therefore, a stimulation protocol comprising 10 odorants at three dilutions plus negative control lasted ∼93 min (Fig. 4D,E), whereas a protocol of 10 odorants repeated 5 times (Fig. 4F,G) required almost 150 min. Because of the length of the imaging/stimulation protocol, two sets of animals were used for the two analyses.

For the spatially localized stimulations, we employed a fast odour-delivery device (Raiser et al., 2017) controlled by a stimulus controller (cRIO-9074 combined with IO module NI-9403, National Instruments, Austin, TX, USA) coupled to LabVIEW

Journal of Experimental Biology (2020) 223, jeb218032. doi:10.1242/jeb.218032

software (National Instruments) custom-written by Stefanie Neupert (Department of Neuroscience, University of Konstanz). The outlet of the olfactometer, a glass tube with a 2 mm inner diameter, was placed at a right angle to the antenna, <1 mm from the antenna at different proximal-to-distal positions (i.e. 6, 12, 18 and 24 mm from the scapus). Given a total antennal length of 40–50 mm, such an experimental configuration would stimulate ∼5% of the antennal length. For each odorant and concentration, three stimuli of 100 ms with 10 s inter-stimulus interval were applied. Odorants were given in a pseudorandomized order; concentrations of odorants were created between 10^{-2} dilution and undiluted (pure). The air carrier flow was set to 1 l min^{-1} and the valve-controlled flow was set to 300 ml min^{-1}, for a total constant flow of 1.6 l min^{-1} (Raiser et al., 2017). Odour arrival, calibrated with a photoionization detector, was 120 ms after trigger onset, corresponding to a 3-frame delay at 25 Hz acquisition rate.

For periplanone B stimulation, we adopted a simplified version of the fast odour delivery device described above to reduce tubing length. A filter paper loaded with 10 µl of purified periplanone B was loaded immediately upstream of a three-way solenoid valve (Lee Products Ltd, Gerrards Cross, UK) controlled by the above-described LabVIEW software. In non-stimulating conditions, the valve received an input of clean air, directed into an air-carrier tube (length 40 mm, internal diameter 3.2 mm, Tygon tubes 2001 ultra-pure, Carl Roth, Karlsruhe, Germany), whose outlet was placed ∼1 mm from the antenna and perpendicular to it in either a proximal (6 mm) or a distal (24 mm) position (Fig. 3A). The air carrier flow was set to 800 ml min^{-1} and the valve-controlled flow was set to 150 ml min^{-1} for a total constant flow of 950 ml min^{-1}. During stimulation, the valve switched from clean air to odour stimulus. For each experiment, we delivered three stimuli of 1 s at t=2, 10 and 18 s.

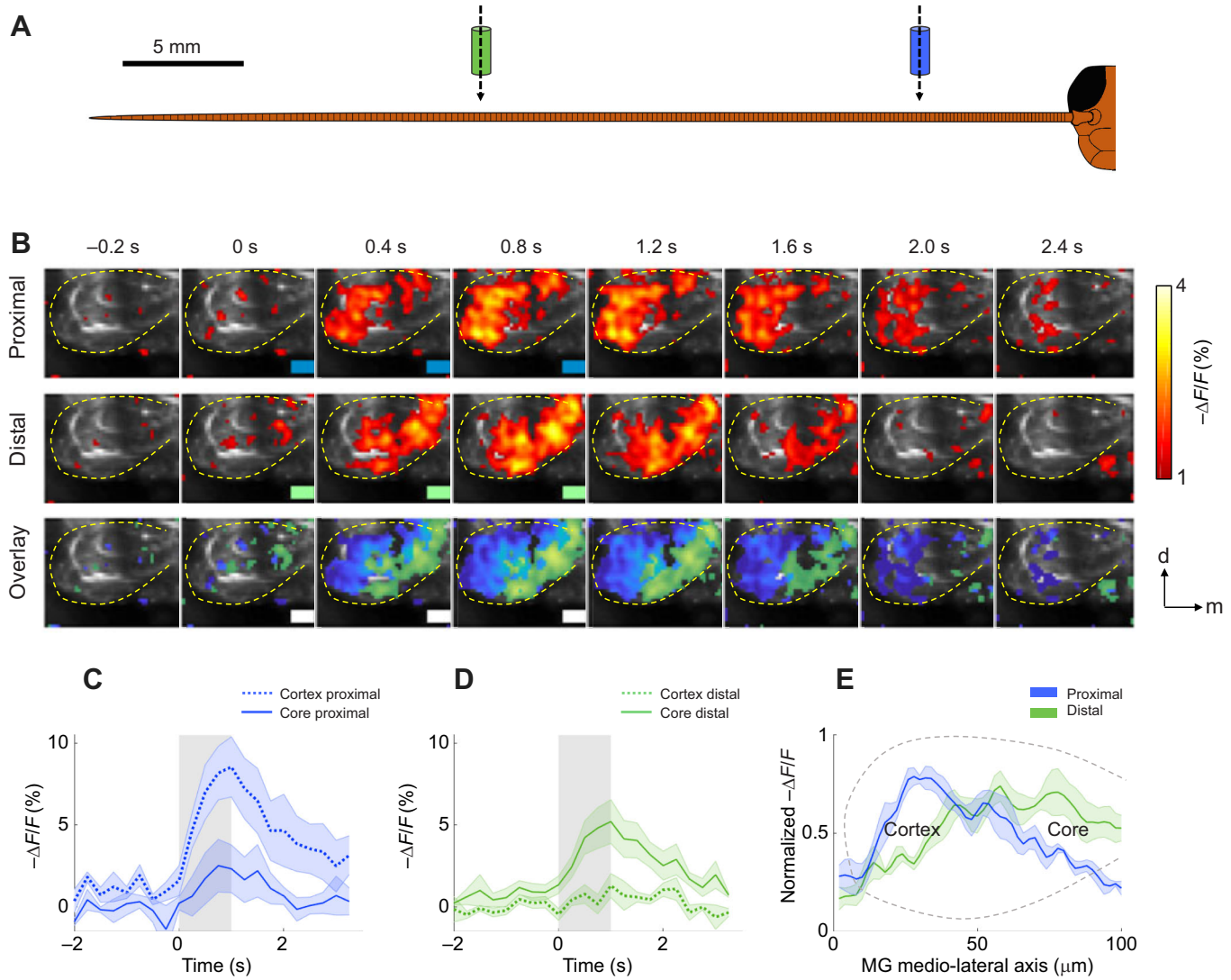

Fig. 3. Antennotopic odour response in the macroglomerulus. (A) Schematic representation of the localized stimulation experiment. Blue, proximal stimulation (6 mm from the scapus); green, distal stimulation (24 mm from the scapus). (B) Time sequence of a representative macroglomerulus (MG) response to proximal and distal periplanone B stimulation. Note how a proximal stimulus activates the (dorso-) lateral area (glomerular cortex), while a distal stimulus activates the (ventro-) medial area (glomerular core), preferentially. The yellow dashed line delimits the MG; green/blue rectangles indicate distal/proximal stimulus delivery. d, dorsal; m, medial. Scale bar: 50 µm. A low cut-off at 1% $\Delta F/F$ (change in fluorescence intensity relative to the resting fluorescence intensity) was applied for response visualization. (C,D) Mean response (±s.e.m., n=4) of MG core (continuous line) and cortex (dotted line) to a proximal (C) and a distal (D) stimulation. (E) Mean evoked responses (±s.e.m., n=4) along the longitudinal MG axis for proximal and distal stimulation, where position 0 µm corresponds to the most lateral side and position 100 µm to the most medial side of the MG. See Fig. S1 for the original traces.

Journal of Experimental Biology (2020) 223, jeb218032. doi:10.1242/jeb.218032

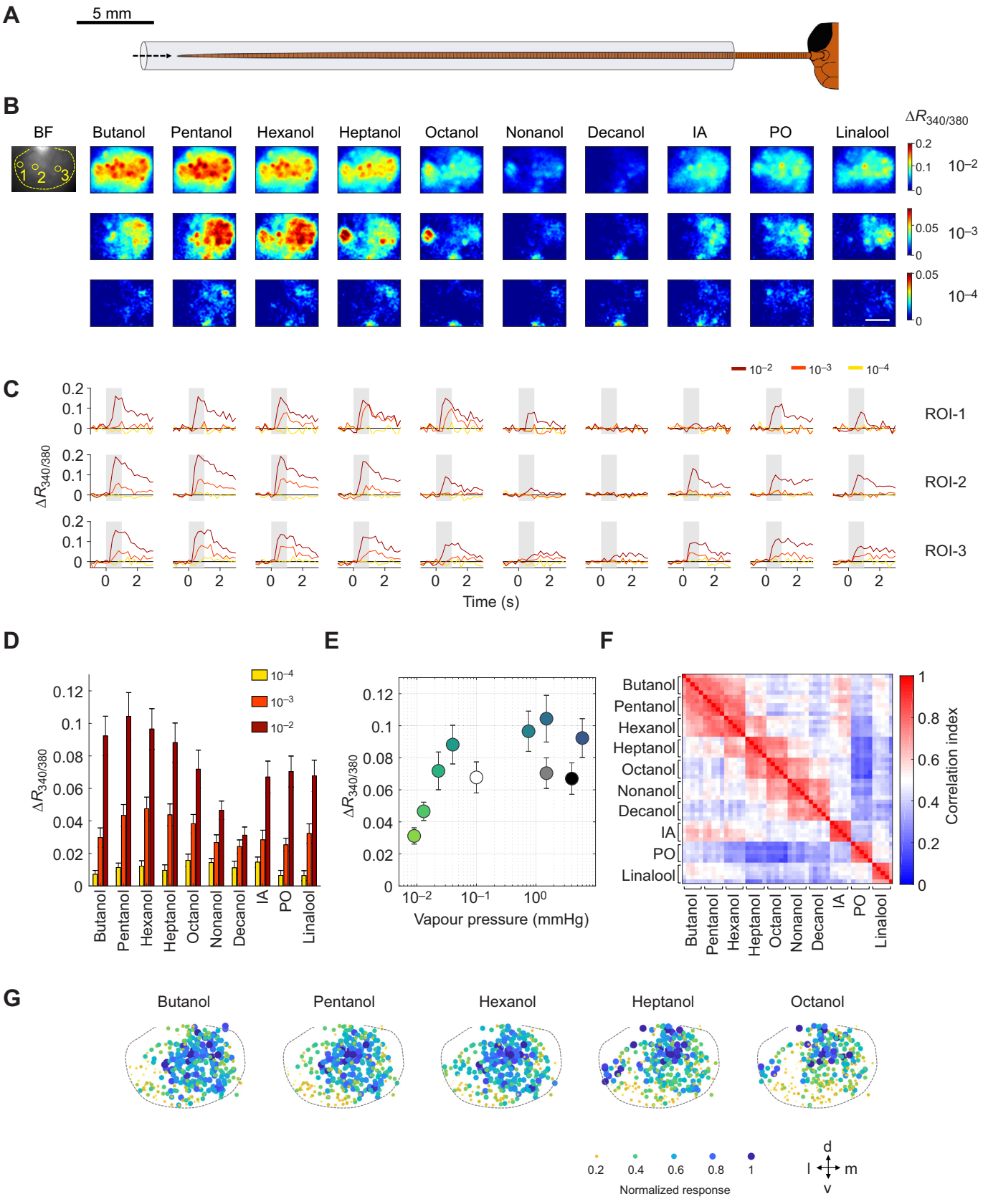

Fig. 4. See next page for legend.

Fig. 4. Common odorants evoke stimulus-specific combinatorial patterns in the AL. (A) Schematic representation of stimulation experiments. The dashed arrow indicates the flow of odour pulses to the antenna through a Teflon tube. (B) Representative spatial panels of evoked responses in one individual for 10 odorants at three dilutions (10^{-1}, 10^{-2}, 10^{-3}). The dashed line in the bright field (BF) image on the left indicates the AL. IA, isoamyl acetate; PO, peppermint oil. Scale bar: 200 µm. (C) Temporal response profiles of the three regions of interest (ROI-1, -2, -3) indicated with yellow circles in the BF image of B. Colours refer to different dilutions; grey bars in the plots indicate the stimulation window. (D) Mean±s.e.m. responses in maximally responsive regions for all odorants and dilutions (n=11). (E) Mean±s.e.m. responses in maximally responsive regions for the 10^{-2} dilution plotted versus odorant vapour pressure (n=11). At the low end (few molecules), responses increased with vapour pressure (increasing number of molecules); at the high end (many molecules), there was no relationship between the two. (F) Correlation analysis among glomerular response vectors of five repetitions of 10 odorants at 10^{-3} dilution. Odorants were delivered in a pseudorandomized order. Mean correlation map for 9 animals. Note how chemically similar odorants elicit physiologically similar response patterns. (G) All odour-induced responses from 9 cockroaches were normalized within each animal and plotted onto a reference AL for a systematic series of aliphatic alcohols ranging from C4 (butanol) to C8 (octanol). Note the gradual shift of main activity along the AL surface. Normalized intensity of the response is encoded by marker colour and size. d, dorsal; v, ventral; l, lateral; m, medial.

Data analysis

Glomerular 3D reconstruction and volumetric analysis (Fig. 2) were conducted with Amira Software (Thermo Fisher Scientific). Analysis of glomerular filling of OSNs was conducted blind: a non-informative code was assigned to each brain sample, and both confocal imaging and 3D reconstruction were conducted without knowing the extent of antenna amputation. Regions of maximal response in the MG (Fig. 3) were automatically defined based on the global response maxima to proximal and distal stimulations. In brief, average response maps to proximal and distal stimuli were segmented using a multilevel threshold (the Otsu algorithm, implemented in Matlab, MathWorks Inc.) to detect the highest activity region >50 pixels (~100 µm^2). As in all tested preparations these were located in the outer and inner part of the MG, respectively, we labelled them as ‘cortex’ and ‘core’. With the wide-field fluorescence microscope, we used a ratiometric protocol for calcium imaging (Fura-2 has excitation wavelengths of 340 and 380 nm and an emission wavelength of 510 nm). Ratios of 340 to 380 nm signals were calculated ($R_{340/380}$), and offset was removed by subtracting the mean signal before odour stimulation ($\Delta R_{340/380}$). To construct odour response maps, we considered the mean activity between 0.6 and 1 s after stimulus onset. Eleven cockroaches were used to assess response sensitivity to the 10 odorants at three dilutions. Thus, each animal was tested with the same set of stimuli, and all comparisons in the plots (Fig. 4D,E) are among independent measures obtained from different animals. Response to the solvent (mineral oil) was subtracted from all stimulus-induced signals. A second set of animals (n=9) was used to assess the specificity of stimulus responses (Fig. 4F) and spatial representation of alcohols in the AL (Fig. 4G). Thus, response correlation matrix and response maps are based on independent measures of 9 animals. For quantifying response maps across the entire AL (Fig. 4G), 42±2 (mean±s.e.m., range 29–50, n=9 cockroaches) responsive areas of 5×5 pixels (corresponding to 19×19 µm) were hand-selected to construct stimulus-specific response vectors. Correlation analysis across response vectors of the same and different stimuli was performed to assess stimulus specificity of the elicited response and odour similarity (Fig. 4G). To assess spatial representation of alcohols with increasing chain length, responses from all animals (n=9) were pooled onto the same meta-antennal lobe. To focus on relative intensity and spatial distribution, all responses from each animal/odorant combination were normalized as: normalized $RI_{g,a,o}=(RI_{g,a,o}-RI_{min,a,o})/(RI_{max,a,o}-RI_{min,a,o})$, where $RI_{g,a,o}$ is the response intensity in a specific area g, and $RI_{min,a,o}$ and $RI_{max,a,o}$ are the minimum and maximum response intensity in the AL of animal a for odorant o. Normalized responses to alcohols were plotted onto a standard AL according to their original coordinates and size in a colour-coded map. For the analysis of responses to stimuli at different locations along the antennae (Fig. 5), a third set (n=14 cockroaches) was used. Amplitude was calculated as mean response intensity between 120 and 280 ms after stimulus onset. To determine response latency, response curves were fitted with the sigmoidal function $f(t)=a/[1+e^{-b(t-c)}]+d$, where a is the amplitude of the fitted curve, $a\times b/4$ is the slope of the sigmoid, c is the time to 50% response and d is the minimum value of the sigmoid. Response latency was defined as the time point along the fitted curve where the intensity value crossed a threshold of 2σ of the pre-stimulus activity. As it is not possible to extract a latency value in the absence of a response, data points in Fig. 5C represent mean and s.e.m. of the latency for those responses strong enough that curves could be fitted. Mean, s.e.m. and n values of each point in Fig. 5C are given in Table S1. Calcium imaging data analysis was conducted with custom-written Matlab scripts (MathWorks Inc.).

Statistical analysis

The relationship between antennal degeneration and OSN glomerular filling (Fig. 2D) was assessed with a linear regression analysis. Responses to proximal/distal stimuli in the MG core/cortex (Fig. 3E) were analysed with Student’s paired t-test. The effect of odorant, dilution and stimulus location on signal intensity and latency (Fig. 5) was assessed with a three-way analysis of variance. The normal distribution of all datasets subject to a parametric statistical test was tested with a one-sample Kolmogorov–Smirnov test. Travelling speed of neural activity along the antenna was calculated for each animal (n=14) by fitting all response latencies for the different odorants, dilutions and locations with a linear regression.

RESULTS

uPNs in the AL: morphology

AL injection with the fluorescent tracer Alexa Fluor 568 revealed the multiple AL PN tracts (Fig. 1A,B, green arrowhead; Movie 1). The neuroanatomy of ALTs is consistent with previous observations (Malun et al., 1993), and was used to guide us in performing selective retrograde labelling, in a protocol adapted from those for other insect species, e.g. honeybees (Sachse and Galizia, 2002) and ants (Zube et al., 2008). A localized tracer injection into the medial tracts ALT-I/II medio-ventral to the MB calices (Fig. 1A,B, blue arrowhead) allowed for uPN population backfilling. Their somata group into two main clusters, type I (Fig. 1Ci) and type II (Fig. 1Cii), located on the antero-dorsal side of the AL (Strausfeld and Li, 1999; Watanabe et al., 2017). Alternatively, dye injection on the ventral side of the LP (Fig. 1A, magenta arrowhead) allowed labelling of mPNs (via the outer-ALT), whose somata localize postero-laterally with respect to the uPN clusters (Fig. 1Cii). Here, we focused on uPN labelling to investigate the basis of olfactory coding in a hemimetabolous insect. After tracer injection, the cell body clusters and their dendritic arborizations within the glomeruli could be easily identified (Fig. 1D; Movie 2). Observation of uPNs labelling confirmed previous studies indicating that each glomerulus is innervated by only one uPN, with the exception of the MG (Schaller, 1978; Watanabe et al., 2017).

Journal of Experimental Biology (2020) 223, jeb218032. doi:10.1242/jeb.218032

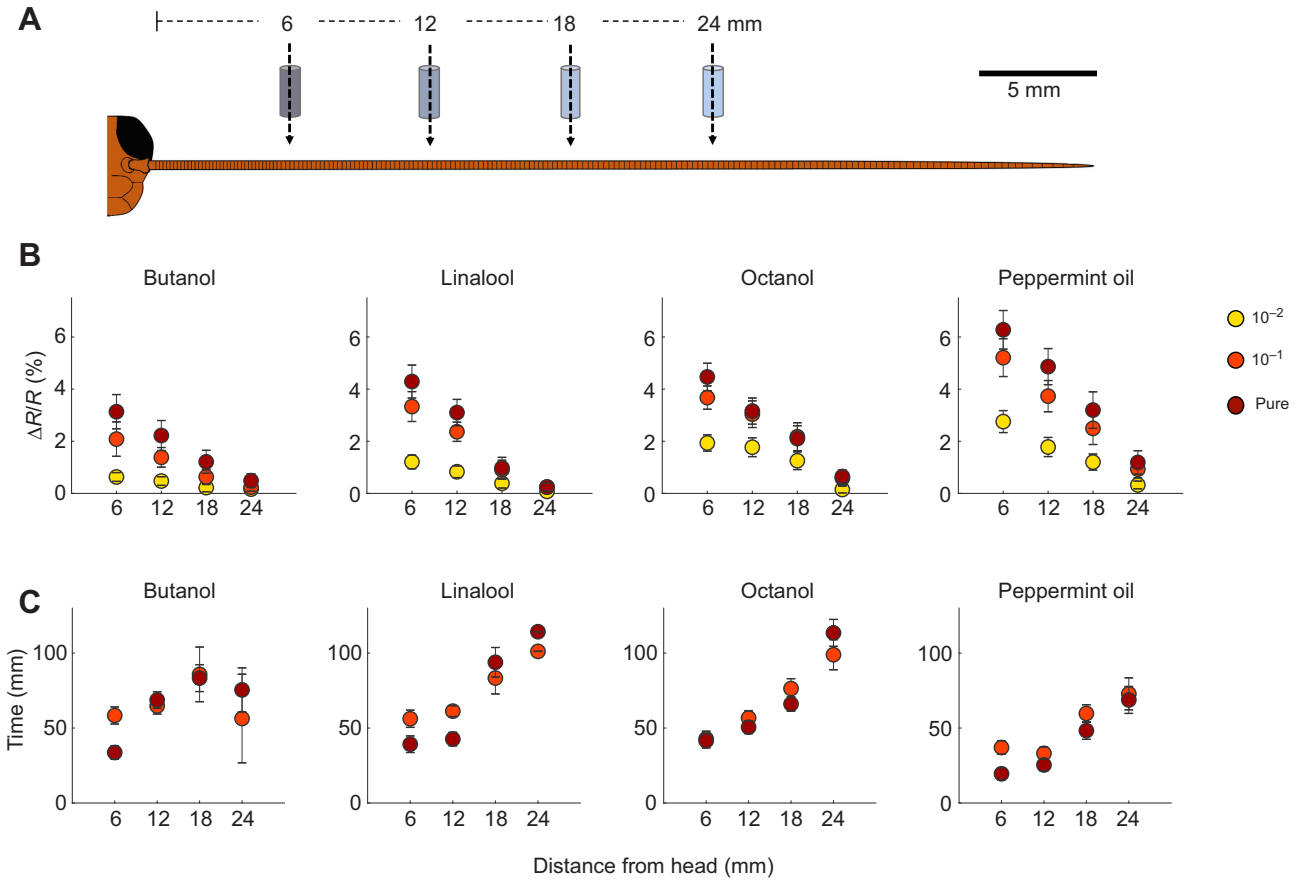

Fig. 5. Analysis of response latency and intensity of spatially localized olfactory stimuli. (A) Schematic representation of localized stimulation experiments. (B) Mean±s.e.m. response intensity (n=14) in the strongest responsive region of the AL for four stimulus locations and three dilutions. In all cases, the response increased as the stimulus was moved closer to the head. (C) Mean±s.e.m. latency of the same strongest responsive regions for four stimulus locations and two dilutions. Latency increased with increasing distance from the head. See Table S1 for n of latency values.

Given that previous work focused on the MG only, we investigated antennotopic innervation in ordinary glomeruli. By removing a distal portion of the antenna (at 0%, 25%, 50%, 75% or 100% of its length), we selectively induced neurodegeneration of the ORNs originating in the missing part. After 7 days, we bulk labelled all remaining sensory axons and evaluated the decrease in OSN-innervated area within randomly selected glomeruli using 3D reconstruction of confocal imaging (Fig. 2). Average intact glomerulus diameter was 45±8 µm, measured from reconstruction of PN staining in n=369 glomeruli (Fig. 2C). From that, using uPN labelling as a counterstain to visualize the intact glomerulus, we could assess OSN innervation volume after partial OSN terminal degeneration. We found that the glomerular volume occupied by OSN terminals was reduced in proportion to the percentage of missing antenna (Fig. 2D) and that OSNs originating in different antennal segments innervated different glomerular compartments (linear regression analysis, R^2=0.43). Interestingly, despite the difference between the number of OSNs in ordinary glomeruli and in the MG, their innervation pattern was conserved (Nishino et al., 2018): OSNs originating on the distal portion of the antenna innervated the portion more proximal to the PN innervation site, whereas OSNs hosted in proximal antennal segments innervated the glomerular region further from the uPNs entry site. Despite this consistent pattern, the detailed distribution showed a high variability across glomeruli (Fig. 2D), indicating that the distribution of receptor types along the antennal flagellum might differ for different receptor types.

Antennotopic odour response in the MG

Antennotopic glomerular innervation provides the means to relay spatial information from along the antennal flagellum to the central nervous system. The male MG responds to the main component of the female sex pheromone periplanone B, and is innervated by multiple spatially segregated uPNs (Hösl, 1990; Nishino et al., 2018). We used this arrangement to test whether the spatial innervation of OSNs leads to spatial information in uPNs, and how odour locations are mapped by the MG uPNs. We used confocal imaging of Fura-2-loaded PNs and compared proximal and distal stimulations (6 and 24 mm from the head; Fig. 3A). We found that, consistent with the anatomical observations, distal stimulations elicited calcium responses in a more medial portion of the MG (‘core’), while proximal ones activated more lateral (‘cortical’) regions (Fig. 3B–E) (Student’s paired t-test, P<0.05, n=4). In addition, proximal stimuli induced stronger responses, whereas distal stimuli consistently elicited weaker ones (Fig. 3C–E; see Fig. S1 for individual traces).

uPN calcium imaging

Next, we investigated how common odorants are represented in the cockroach’s AL. The selected odour panel included nine monomolecular odorants and a complex plant extract, peppermint oil. Such odorants have previously been used for cockroaches in both electrophysiological and behavioural assays (Arican et al., 2019; Boeckh and Ernst, 1987; Gehret et al., 2001; Lemon and

Journal of Experimental Biology (2020) 223, jeb218032. doi:10.1242/jeb.218032

Getz, 1997; Matsumoto et al., 2012; Sakura and Mizunami, 2001; Sakura et al., 2002). Although not all are necessarily frequent in the natural environment of this species, their ability to induce clear and robust activity patterns in the AL provides an important tool for our comprehension of the coding properties of the cockroach AL. Medial PN tracts were retrogradely filled with the calcium-sensitive dye Fura-2. Successful labelling resulted in bright fluorescence of the cell bodies and dendritic arborizations (Fig. 1D; Movie 2), and allowed calcium imaging during olfactory stimulation for several hours. Before stimulation, spontaneous changes in calcium amplitude could be observed in discrete areas, comparable in size and shape to individual glomeruli. During stimulation (see schematic diagram in Fig. 4A), fluorescence changes were observed in these discrete areas, as well as in larger portions of the AL, suggesting that in some instances, clusters of neighbouring glomeruli were activated simultaneously (Movie 3). Because it was not possible to reliably identify individual glomeruli across animals, we compared odorant- and concentration-induced response maps within individuals, and extracted general coding features from an across-individual comparison. Eleven cockroaches were tested with a panel of 10 odorants at three dilutions (10^{-2}, 10^{-3} and 10^{-4}). Response intensity was stimulus dependent, with long-chain alcohols (1-nonanol and 1-decanol) inducing much weaker responses than shorter-chain ones (1-butanol to 1-heptanol). Other tested compounds (1-octanol, linalool, isoamyl acetate and peppermint oil) induced concentration-dependent robust responses, with smaller amplitudes than for short-chain alcohols. Fig. 4B provides a representative panel of odour response maps. Each image (600×450 µm) shows the anterior view of the right AL. Within the responsive area, spherical spots of activity of ∼45 µm in diameter were clearly visible, probably corresponding to activated AL glomeruli. Different odour concentrations were tested to investigate the sensitivity of the cockroach's olfactory system, and clear stimulus-induced responses were obtained for high and medium concentrations, whereas no response above that to the negative controls were observed for 10^{-4} dilutions (Fig. 4B,C). This effect was consistent across all tested odorants. For all odorants, spatial response patterns at lower dilutions were confined to smaller areas. Accordingly, different glomeruli had odorant-specific concentration–response curves. For instance, as shown in Fig. 4C, regions of interest ROI-1 and ROI-3 responded with similar intensity to butanol at 10^{-2} dilution, but while ROI-3 responded at a level of 10% to stimulation with 10^{-3} dilution of 1-butanol, ROI-1 was silent at this concentration. Similarly, 10^{-2} linalool triggered a comparable response in ROI-2 and ROI-3, whereas at 10^{-3} dilution the activity it induced in ROI-3 was half that at the highest concentration, while ROI-2 was non-responsive.

For each odour response map, we considered the area with the strongest activity to estimate odorant and concentration sensitivity across animals. For each odorant/dilution pair, we computed a mean response value (n=11 animals). Overall, cockroach uPNs displayed a response of 0.07–0.11 $\Delta R_{340/380}$ in response to odour stimulations at 10^{-2} dilution (a lower response for long-chain alcohols), 0.02–0.05 $\Delta R_{340/380}$ to intermediate dilution and 0.01–0.02 $\Delta R_{340/380}$ to 10^{-4} dilution (Fig. 4D). The number of molecules in a stimulus scales, to a large degree, with its vapour pressure. Fig. 4E illustrates the relationship between odorant vapour pressure and AL activity. We observed a decrease in responsiveness for long-chain alcohols, which have the lowest vapour pressure of the tested odorants. However, for the other odorants, we found comparable response intensities to molecules with very different vapour pressures. For instance, responses elicited by 1-octanol and 1-butanol, whose vapour pressures differ by 260-fold (6 versus 0.023 mmHg), were comparable. Similarly, isoamyl acetate, peppermint oil and linalool, despite having different vapour pressures (0.1, 1.5 and 4.0 mmHg, respectively) evoked responses of comparable intensity (Fig. 4E). Thus, at least for some stimuli, the olfactory system appears to compensate for vapour pressure, i.e. for expected molecule density in the odour plume.

Physiological odour similarity can be assessed by measuring the correlation coefficient between odour response maps (Guerrieri et al., 2005). With this purpose, we exposed a new group of cockroaches (n=9) to five repetitions of 10 odorants at an intermediated dilution (10^{-3}) in a pseudorandomized order. For each animal, we constructed stimulus–response vectors considering all functional units activated by any of the odorants. We obtained 50 vectors from five repetitions of 10 odorants, and calculated a correlation matrix across all vectors to quantify odour–response similarity. We found that responses to repetitions of the same stimulus were highly correlated (Fig. 4F), whereas responses to different odorants showed different degrees of similarity. Interestingly, chemically similar alcohols showed higher correlation values than chemically dissimilar ones (based on carbon chain length). How is the 'chain length' parameter represented across the cockroach's glomerular space? To answer this question, we mapped the responsive areas from all individuals and overlaid them onto a common reference AL. Then, we analysed the spatial distribution of the observed responsive glomeruli for the chosen alcohol series, with the exclusion of 1-nonanol and 1-decanol because of the generally low responses to them (Fig. 4G). Notably, a cluster of strongly responsive glomeruli in the central part of the AL was present for all alcohols. However, short-chain alcohols tended to activate more central/medial regions of the AL, whereas with increasing chain length, the responsive area shifted from centro-medial to centro-lateral.

Representation of spatially confined stimuli

With the previous set of experiments, we considered the antenna as a whole, and stimulated the entire array of OSNs. However, OSNs that express the same olfactory receptor maintain an antennotopic organization within the glomeruli (Fig. 2). To investigate how spatially confined stimuli are encoded in the AL, we used short stimulations and a narrow olfactometer outlet placed perpendicular to the antenna at different locations, i.e. at 6, 12, 18 and 24 mm from the scapus (olfactometer inner diameter, 2 mm; distance from antennal surface, <1 mm; see schematic diagram in Fig. 5A). We selected 24 mm as the most distal position because more distal stimuli rarely produced detectable responses. For this experiment, we employed four odorants, eliciting strong and clear responses: a short-chain (1-butanol) and a long-chain alcohol (1-octanol), linalool and peppermint oil. In addition, three dilutions were used: pure odorants, and 10^{-1} and 10^{-2} dilution. This experimental design required lower odorant dilutions than before because of its high spatial and temporal confinement. For each odour/dilution/position/animal combination, we considered the region of the AL with the strongest stimulus-induced response, and analysed its response intensity and latency. Response intensity (Fig. 5B) depended on the odorant (three-way ANOVA, d.f.=3, F=19.79, P<0.01), concentration (d.f.=2, F=44.28, P<0.05) and stimulus location (d.f.=3, F=48.75, P<0.01), with proximal stimuli generating stronger responses than distal ones. Notably, significant interactions were found between the factors concentration and position (d.f.=6, F=4.33, P<0.01), underlining the fact that a significant effect of concentration on the elicited response depends on the position effect (i.e. at distal locations, responses are weaker

and concentration-dependent differences cannot be observed). To quantify response latency (Fig. 5C), we fitted the rising part of the response profile with a sigmoidal curve and considered as response onset the time point of crossing a threshold of two standard deviations from baseline activity. For this, we only used the two strongest concentrations, whose responses were robust enough to provide reliable data fitting, and observed that latency increased with distance from the head. In this case, the sole factor influencing response latency was stimulus location (d.f.=3, F=7.76, P<0.01), while odorant (d.f.=3, F=2.04, P=0.11) and concentration (d.f.=1, F=0.51, P=0.47) had no significant effect. We performed a linear regression for stimulus location to assess propagation speed along the antenna. Mean (±s.e.m.) OSNs conduction velocity was 0.37±0.04 m s^{-1}, ranging from 0.19 to 0.58 m s^{-1} across animals (n=14 preparations), with a delay of 30±16 ms between the stimulation of the most proximal antennal section and the first detectable evoked activity in the AL PNs. Considering that a proximal stimulation elicits OSN activity at ∼7 mm from the AL, and that such activity travels along the antennal nerve at 0.37 m s^{-1}, it will reach the AL with a latency of ∼19 ms. Our observation that a proximal stimulation induces AL activity with ∼30 ms time delay suggests that the average lag between the OSN input signal and a detectable calcium activity in the AL output neurons is approximately 11 ms. In a recent study, Egea-Weiss et al. (2018) were able to quantify OSN response latency in the fruit fly, showing that OSN response time may be as fast as 3 ms from odour arrival. In addition, it has been reported that other insects (i.e. hissing cockroach, locust, silk moth and honeybee) also have a OSN response latency of a few milliseconds after stimulus arrival (Szyszka et al., 2014). Assuming that the American cockroach OSNs have similar response dynamics, our analysis suggests that an olfactory input needs approximately 8 ms to be processed within its AL network.

DISCUSSION

The olfactory circuit of *P. americana* has been extensively investigated thanks to its robustness and accessibility for long-term electrophysiology and neuronal tracing (Ernst and Boeckh, 1983; Hösl, 1990; Husch et al., 2009; Malun et al., 1993; Salecker and Boeckh, 1996). Hence, being amongst the best-described olfactory systems, it provides an excellent model for investigating how a hemimetabolous insect encodes odorants. In addition, the cockroach's extremely long antennae, in both absolute and relative terms, offer the opportunity to study whether and how spatial information of odorants is encoded in the AL. With this in mind, we set out here to assess how stimulus nature, concentration and spatial location are mapped within the cockroach olfactory system.

Coding similarity across insect species

In hemimetabolous insects, at least two different solutions exist for the glomerular organization of the AL: the American cockroach has a comparatively small number of large glomeruli and uPNs (Watanabe et al., 2010), which is similar to the arrangement in many holometabolous insects studied so far, such as fruit flies (Grabe et al., 2015; Laissue et al., 1999), honeybees (Galizia et al., 1999a), moths (Hildebrand et al., 1979) and red flour beetles (Dreyer et al., 2010), but also in some hemimetabolous species, such as the heteropteran bug *Euschistus heros* (Kristoffersen et al., 2008); locusts, however, have a high number of microglomeruli, and only mPNs (Hansson et al., 1996; Moreaux and Laurent, 2007). The question arises, therefore, whether the cockroach AL has a functional organization that is similar to the one observed in several holometabolous insects or instead to the more closely related locust.

Selective labelling of AL PNs was initially developed for the honeybee (Sachse and Galizia, 2002) and later adapted to other species. For the first time, we were able to transfer this method to a hemimetabolous insect, thus opening the way for comparative investigations of odour coding in holometabolous versus hemimetabolous insects. This has allowed us to increase the number of insect species for which we can investigate the logic of olfactory coding, and to define essential common features in the ways in which volatile molecules are detected and processed: differences in architecture and physiology of these two insect groups would indicate on alternative evolutionary mechanisms for probing an olfactory environment; alternatively, common mechanisms would indicate a likely common origin of the underlying architecture.

One of the advantages of uPN backfilling is the possibility of monitoring a major part of the AL population all at once. This allows the construction of broad response maps to study how different olfactory stimuli are spatially represented in the AL. A further advantage of this method in the American cockroach is that in this species each glomerulus is innervated by a single uPN (Ernst and Boeckh, 1983). As a consequence, all measured glomerular responses reflect the activity of exactly one neuron. Thus, differences in signal strength or quality across glomeruli cannot be attributed to the activation (or labelling) of a different number or proportion of neurons. Successful staining resulted in the clear labelling of the uPNs, with their somata clusters in the dorso-lateral region of the AL (Fig. 1; Movie 2).

Calcium imaging analysis allowed us to measure how olfactory stimuli are represented in the AL within and across individuals. In agreement with the logic of a combinatorial code – described in holometabolous insects such as moths (Carlsson et al., 2002; Galizia et al., 2000), honeybees (Sachse et al., 1999) and fruit flies (Fiala et al., 2002; Silbering et al., 2008), and also in *Periplaneta* – each odorant induced the selective activation of a subset of AL glomeruli. Within a single individual, glomerular response maps were stimulus specific and reproducible, as shown by our correlation analysis (Fig. 4F). Testing different odorant dilutions revealed a concentration dependency of the elicited activity in terms of both intensity (stronger stimuli induced stronger responses) and responsive areas (stronger stimuli activated more glomeruli). In our analysis, we did not observe areas of the AL responsive to low but not to high odorant concentrations. Studies on the honeybee (Sachse et al., 1999), moth (Meijerink et al., 2003) and fruit fly (Couto et al., 2005) have shown that chemical properties such as the alcohol chain length or functional groups can be encoded by a chemotopic glomerular response map. In particular, alcohols with similar chain lengths induce partially overlapping activity patterns, suggesting not only that chemically related odorants evoke similar activity patterns but also that chemical features (e.g. chain length, functional group) are not encoded by a single glomerulus but rather by a glomerular ensemble. Uchida et al. (2000) were able to isolate glomerular domains in the rat olfactory bulb responding to particular functional groups. This would suggest that even if a chemical feature is not efficiently encoded by a single glomerulus, it may still be encoded by glomerular afferents to a spatially confined domain of the olfactory bulb. To probe whether this coding logic also applies to the American cockroach, we tested the neural representation of a series of aliphatic alcohols with increasing chain length. A correlation analysis performed on the evoked response maps revealed that alcohols with similar length generated more similar glomerular response patterns (Fig. 4F). In addition, superimposing glomerular activity from different animals onto a

reference AL revealed a shift in the response maps from a ventro-medial to a more dorso-lateral region of the AL upon stimulation with short- to long-chain alcohols (Fig. 4G). Thus, there is a topological mapping of the chemical structure (here: chain length) onto the AL geometry. These findings are consistent with previous observations in certain holometabolous insects such as the honeybee or the fruit fly, and indicate that, despite the divergent evolutionary history, the logic behind olfactory coding inferred from holometabolous insects may also apply to (at least some) hemimetabolous ones.

Olfactory systems in animals follow two tasks: (1) generate an olfactory space that can accommodate almost any odorant, and (2) identify ecologically relevant substances, often with very high sensitivity. The first is accomplished by a combinatorial encoding logic in most species studied so far, the second by dedicated, highly sensitive olfactory receptors in labelled lines (Galizia, 2014; Grabe and Sachse, 2018). Combinatorial coding is best demonstrated by using substances that span a chemical logic, such as aliphatic alcohols (Sachse et al., 1999). Here, we show that the cockroach encodes aliphatic alcohols by activating overlapping populations of glomeruli, a clear hallmark of combinatorial coding (Fig. 4). Labelled lines are more difficult to identify, because the substances that are encoded are often species specific, such as sexual pheromones. Here, we used the sexual pheromone periplanon B to investigate a labelled line system, and how space is encoded therein (Fig. 3). Recent work has revealed an increasing number of cases where individual chemicals, such as geosmin or iridomyrmecin, were encoded by specific receptors in insects (Ebrahim et al., 2015; Stensmyr et al., 2012). The interplay of dedicated circuits and overlapping combinatorial coding has also been shown in the lepidopteran *Manduca sexta*, where glomeruli are spatially organized by behavioural relevance (Bisch-Knaden et al., 2018). More research will be needed to test whether dedicated, highly selective sensory channels also exist in the cockroach, and where they would be located within the AL.

Encoding of spatial olfactory information

The American cockroach is endowed with extremely long segmented antennae, such that different antennal segments are sufficiently apart to experience different olfactory environments. Having access to receptors along the full length of a flagellum can, in principle, provide several types of information: (1) the movement of a plume towards or away from the animal could be sensed; (2) the concentration gradient along the antenna could be detected – a relevant feature given that cockroaches live in shelters, where air turbulence is low and concentration gradients may be important; (3) the spatial structure of an odour plume could be analysed, i.e. whether the plume is spatially uniform (indicating a single odorant source) or spatially complex (indicating distinct odorant sources). The long antennae make the cockroach an ideal model for investigating whether and how the spatial structure of an olfactory stimulus could be encoded. One hypothesis would be that there is antennotopic mapping, i.e. that the brain maintains the information of proximal and distal olfactory receptors separate. In this case, we would expect a spatial segregation of proximal and distal innervation, and a mechanism to maintain that separation to higher order brain centres. An alternative hypothesis would be that spatial information is extracted through active sensing; that is, by sweeping antennae in space and proprioceptive analysis of antennal position. In this case, we would expect the highest sensitivity of the antenna to be in the distal segments, which become the most important segments for spatial analysis. A recent report from Nishino et al. (2018) revealed that the cockroach MG is innervated by a group of PNs with an ordered subglomerular morphology. By means of single-cell electrophysiology, they showed that each MG PN responds to a restricted antennal region. Here, by monitoring the activity across all MG uPNs at once, we tested the consequences of this finding. Our observations are consistent with the model of a functionally antennotopical glomerular organization, and show that distal stimuli induced stronger responses in the medial portion of the MG (i.e. close to the entry site of uPNs into the MG), whereas proximal stimulations resulted in a lateral/cortical MG activation. This finding complements the previous report (Nishino et al., 2018) showing that glomeruli are not the smallest unit of olfactory processing, but that subglomerular structures may convey information about stimulus location along the antennae. In addition, we observed that distal stimuli have a tendency to elicit weaker responses than proximal stimuli. Even if not statistically significant, this observation is coherent with previous electrophysiological observations, which showed that uPNs responsive to distal pheromone stimuli respond with about 60% (Hösl, 1990) or 75% (Nishino et al., 2018) of the intensity of uPNs responsive to proximal stimuli. This effect is probably due to a decrease in sensillar density along the cockroach antenna, and thus to a smaller population of responsive neurons (Hösl, 1990; Watanabe et al., 2018).

Can the spatial arrangements of other common odorants be encoded by a similar mechanism in other (‘ordinary’) glomeruli? Our study shows that the sensitivity to common odorants – different from the sensitivity to periplanone B – decreases drastically along the antenna. With calcium imaging analysis, we could detect a clear response to a plume of odorant localized a few millimetres from the head, but almost no activity when the odour plume was presented to a more distal antennal section. This effect can be explained only partially by the decrease in sensillar density along the antenna from proximal to distal (Hösl, 1990; Watanabe et al., 2018). Indeed, olfactory sensilla density may explain up to a 2-fold decrease in sensitivity along the antenna, but not the 5- to 10-fold signal decrease that we observed (Fig. 5). Such a low sensitivity in the distal portion of the antenna suggests that spatial analysis along the antenna might be more important for the cockroach than proprioceptive analysis of a moving antenna. However, this does not exclude the possibility that the two mechanisms may be used in parallel or in different ecological contexts. In our experiments, antennae were immobilized in order to control stimulus location and to avoid movement artefacts. It may be that proprioceptive analysis has a modulatory effect on AL activity, i.e. that distal stimulation would elicit stronger responses in the AL if (and only if) the antennae were moving.

Most odour molecules interact with multiple ORN types with different affinities, activating multiple glomeruli across the AL. However, different from the MG, ordinary glomeruli are not equipped with multiple uPNs with stereotyped subglomerular morphology, such that all cognate OSNs terminate onto a single uPN. Thus, if the spatial arrangement of an odorant plume could be perceived by the cockroach olfactory system, it is unlikely that it relies on the same mechanism expressed by the MG, because each single uPN per glomerulus could not encode the stimulus location of common odorants. Glomerular subcompartments (and thus antennotopic position of the stimulus) may, however, be encoded by other AL neurons such as local interneurons or mPNs. Indeed, each glomerulus is innervated by multiple mPNs, which do not always innervate the whole glomerulus, but rather ramify in restricted subglomerular portions (Malun et al., 1993). This type of architecture is reminiscent of the spatial coding arrangement

observed for uPNs in the MG (Nishino et al., 2018). In the MG, a large receptive field uPN (L1) covers the entire MG volume, while multiple small receptive field uPNs cover limited portions of the MG. In the rest of the AL, each glomerulus is fully innervated by one uPN (in analogy with the L1-PN system for the MG), while multiple mPNs innervate several glomeruli, although only partially (in analogy with the small receptive field PNs found in the MG, but spatially distributed across multiple glomeruli). In order to test this hypothesis, future studies of mPN single-cell labelling and electrophysiology are required. If, indeed, spatial analysis were performed by mPNs, this would create an interesting dichotomy in odour coding, with a segregation of information across different tracts: space would be coded in mPNs and travel along the lateral ALTs, while odour quality would be coded across uPNs, and travel within the medial ALTs. Similar parallel systems are present across insects and sensory modalities (Galizia and Rössler, 2010).

Spatial and temporal signal integration

Two odorants, A and B, originating from the same source are likely to travel within the same odour plume (Nowotny et al., 2013; Stierle et al., 2013). If such a homogeneous plume crosses the antenna, the same odorant mixture will be experienced by the whole antenna in the same way, triggering the activation of the receptors for A and for B at the same annuli, in synchrony. Hence, the information of the activated OSN population will reach the AL with the same latency, producing a glomerular response map for the synchronous odour object AB. Conversely, if odours A and B originate from different sources, they will result in an asynchronous plume, where components A and B do not travel in synchrony, and reach the antenna at different locations and at different times. Thus, the experience of an asynchronous mixture will evoke the activity of two different OSN ensembles in different spatial and/or temporal locations (one for odorant A and one for odorant B), which will reach the AL with different latencies, depending on the spatio-temporal separation of the two sources. In this second case, a dynamic response map would arise, with a glomerular code shifting from the most proximal component, e.g. A, to the most distal one, e.g. B. In our analysis, we found that a stimulus in a certain portion of the antenna induced a response in the AL PNs, whose latency was a function of the axonal length of the activated OSNs, with a travelling speed of ∼0.37 m s^{-1}. Thus, a stimulus separation of 40 mm along the antennal surface would produce a delay greater than 100 ms in uPNs response time. Estimates obtained from moth PNs show that multiple signals can be temporally integrated when separated by less than 60–80 ms (Tabuchi et al., 2013). This means that two stimuli far apart on the antenna may not be subject to temporal integration, thus supporting the hypothesis that a long antenna would allow for instantaneous discrimination of synchronous versus asynchronous mixtures (Nowotny et al., 2013; Stierle et al., 2013).

Concluding remarks

In conclusion, we show that glomeruli are complex functional units with a subglomerular structure, and suggest that this arrangement may contribute to the ability to encode spatial information of olfactory stimuli. While we confirmed that space along the antenna is maintained as space within the MG, further studies are required to fully understand whether and how information provided by the antennotopic arrangement of non-pheromone receptors is maintained within the brain. We show that in the American cockroach, odour quality, odour concentration and chemical similarity follow a combinatorial logic comparable to what is found in holometabolous insects and in mammals. Finally, proximal antennal segments induce stronger signals in the AL, whereas the distal half of the antenna evokes very weak calcium responses, raising new questions about how the cockroach uses its characteristic long antennae in olfactory coding and active sensing. Further studies, including calcium imaging in mPNs, will help us to elucidate olfactory coding across species.

Acknowledgements

Thanks to Mark Willis for the periplanone samples. Thanks to Stephanie Neupert for experimental control software, to Alina Hebling for assistance in calcium imaging experiments, and to Silvio Widmer for assistance in the volumetric analysis of AL glomeruli.

Competing interests

The authors declare no competing or financial interests.

Author contributions

Conceptualization: M.P., C.G.G.; Methodology: M.P., H.N., E.C.-F., C.G.G.; Formal analysis: M.P., E.C.-F.; Investigation: M.P.; Resources: C.G.G.; Data curation: M.P.; Writing - original draft: M.P.; Writing - review & editing: M.P., H.N., E.C.-F., C.G.G.; Visualization: M.P.; Supervision: H.N., C.G.G.; Project administration: C.G.G.; Funding acquisition: C.G.G.

Funding

This work was funded by the Deutsche Forschungsgemeinschaft Centre of Excellence 2117 ‘Centre for the Advanced Study of Collective Behaviour’ (ID: 422037984).

Data availability

The supplementary movies can also be downloaded at http://neuro.uni.kn/Paoli2020.

Supplementary information

Supplementary information available online at http://jeb.biologists.org/lookup/doi/10.1242/jeb.218032.supplemental

References

Arican, C., Bulk, J., Deisig, N. and Nawrot, M. P. (2019). Cockroaches show individuality in learning and memory during classical and operant conditioning. *Front. Physiol.* **10**, 1539. doi:10.3389/fphys.2019.01539

Bisch-Knaden, S., Dahake, A., Sachse, S., Knaden, M. and Hansson, B. S. (2018). Spatial representation of feeding and oviposition odors in the brain of a hawkmoth. *Cell Rep.* **22**, 2482-2492. doi:10.1016/j.celrep.2018.01.082

Boeckh, J. and Ernst, K.-D. (1987). Contribution of single unit analysis in insects to an understanding of olfactory function. *J. Comp. Physiol. A* **161**, 549-565. doi:10.1007/BF00603661

Borst, A. and Heisenberg, M. (1982). Osmotropotaxis in Drosophila melanogaster. *J. Comp. Physiol. A* **147**, 479-484. doi:10.1007/BF00612013

Brandt, R., Rohlfing, T., Rybak, J., Krofczik, S., Maye, A., Westerhoff, M., Hege, H.-C. and Menzel, R. (2005). Three-dimensional average-shape atlas of the honeybee brain and its applications. *J. Comp. Neurol.* **492**, 1-19. doi:10.1002/cne.20644

Carlsson, M. A., Galizia, C. G. and Hansson, B. S. (2002). Spatial representation of odours in the antennal lobe of the moth Spodoptera littoralis (Lepidoptera: Noctuidae). *Chem. Senses* **27**, 231-244. doi:10.1093/chemse/27.3.231

Couto, A., Alenius, M. and Dickson, B. J. (2005). Molecular, anatomical, and functional organization of the Drosophila olfactory system. *Curr. Biol.* **15**, 1535-1547. doi:10.1016/j.cub.2005.07.034

Distler, P. G. and Boeckh, J. (1997). Synaptic connections between identified neuron types in the antennal lobe glomeruli of the cockroach, Periplaneta americana: II. Local multiglomerular interneurons. *J. Comp. Neurol.* **383**, 529-540. doi:10.1002/(SICI)1096-9861(19970714)383:4<529::AID-CNE9>3.0.CO;2-4

Dreyer, D., Vitt, H., Dippel, S., Goetz, B., El Jundi, B., Kollmann, M., Huetteroth, W. and Schachtner, J. (2010). 3D standard brain of the red flour beetle Tribolium castaneum: a tool to study metamorphic development and adult plasticity. *Front. Syst. Neurosci.* **4**, 1-13. doi:10.3389/neuro.06.003.2010

Ebrahim, S. A. M., Dweck, H. K. M., Stökl, J., Hofferberth, J. E., Trona, F., Weniger, K., Rybak, J., Seki, Y., Stensmyr, M. C., Sachse, S. et al. (2015). Drosophila avoids parasitoids by sensing their semiochemicals via a dedicated olfactory circuit. *PLoS Biol.* **13**, e1002318. doi:10.1371/journal.pbio.1002318

Egea-Weiss, A., Renner, A., Kleineidam, C. J. and Szyszka, P. (2018). High precision of spike timing across olfactory receptor neurons allows rapid odor coding in Drosophila. *iScience* **4**, 76-83. doi:10.1016/j.isci.2018.05.009

Ernst, K. D. and Boeckh, J. (1983). A neuroanatomical study on the organization of the central antennal pathways in insects. III. Neuroanatomical characterization of physiologically defined response types of deutocerebral neurons in Periplaneta americana. *Cell Tissue Res.* **229**, 1-22. doi:10.1007/BF00217877

Fiala, A., Spall, T., Diegelmann, S., Eisermann, B., Sachse, S., Devaud, J.-M., Buchner, E. and Galizia, C. G. (2002). Genetically expressed cameleon in Drosophila melanogaster is used to visualize olfactory information in projection neurons. *Curr. Biol.* **12**, 1877-1884. doi:10.1016/S0960-9822(02)01239-3

Fusca, D., Husch, A., Baumann, A. and Kloppenburg, P. (2013). Choline acetyltransferase-like immunoreactivity in a physiologically distinct subtype of olfactory nonspiking local interneurons in the cockroach (periplaneta americana). *J. Comp. Neurol.* **521**, 3556-3569. doi:10.1002/cne.23371

Galizia, C. G. (2014). Olfactory coding in the insect brain: data and conjectures. *Eur. J. Neurosci.* **39**, 1784-1795. doi:10.1111/ejn.12558

Galizia, C. G. (2018). Neuroscience: an Olfactory Homunculus in the Insect Brain. *Curr. Biol.* **28**, R227-R229. doi:10.1016/j.cub.2018.01.058

Galizia, C. G. and Rössler, W. (2010). Parallel olfactory systems in insects: anatomy and function. *Annu. Rev. Entomol.* **55**, 399-420. doi:10.1146/annurev-ento-112408-085442

Galizia, C. G., McIlwrath, S. L. and Menzel, R. (1999a). A digital three-dimensional atlas of the honeybee antennal lobe based on optical sections acquired by confocal microscopy. *Cell Tissue Res.* **295**, 383-394. doi:10.1007/s004410051245

Galizia, C. G., Sachse, S., Rappert, A. and Menzel, R. (1999b). The glomerular code for odor representation is species specific in the honeybee Apis mellifera. *Nat. Neurosci.* **2**, 473-478. doi:10.1038/8144

Galizia, C. G., Sachse, S. and Mustaparta, H. (2000). Calcium responses to pheromones and plant odours in the antennal lobe of the male and female moth Heliothis virescens. *J. Comp. Physiol. A Sens. Neural Behav. Physiol.* **186**, 1049-1063. doi:10.1007/s003590000156

Gehret, M. J., Appel, A. G. and Tanley, M. J. (2001). Repellency and toxicity of mint oil to American and German cockroaches (Dictyoptera: Blattidae and Blattellidae). *J. Agric. Urban Entomol.* **18**, 149-156.

Gomez-Marin, A., Duistermars, B. J., Frye, M. A. and Louis, M. (2010). Mechanisms of odor-tracking: multiple sensors for enhanced perception and behavior. *Front. Cell. Neurosci.* **4**, 6. doi:10.3389/fncel.2010.00006

Grabe, V. and Sachse, S. (2018). Fundamental principles of the olfactory code. *Biosystems* **164**, 94-101. doi:10.1016/j.biosystems.2017.10.010

Grabe, V., Strutz, A., Baschwitz, A., Hansson, B. S. and Sachse, S. (2015). Digital in vivo 3D atlas of the antennal lobe of Drosophila melanogaster. *J. Comp. Neurol.* **523**, 530-544. doi:10.1002/cne.23697

Guerrieri, F., Schubert, M., Sandoz, J.-C. and Giurfa, M. (2005). Perceptual and neural olfactory similarity in honeybees. *PLoS Biol.* **3**, e60. doi:10.1371/journal.pbio.0030060

Hansson, B. S., Ochieng, S. A., Grosmaitre, X., Anton, S. and Njagi, P. G. N. (1996). Physiological responses and central nervous projections of antennal olfactory receptor neurons in the adult desert locust, Schistocerca gregaria (Orthoptera: Acrididae). *J. Comp. Physiol. A Sens. Neural Behav. Physiol.* **179**, 157-167. doi:10.1007/BF00222783

Hildebrand, J. G. and Shepherd, G. M. (1997). Mechanisms of olfactory discrimination: converging evidence for common principles across phyla. *Annu. Rev. Neurosci.* **20**, 595-631. doi:10.1146/annurev.neuro.20.1.595

Hildebrand, J. G., Hall, L. M. and Osmond, B. C. (1979). Distribution of binding sites for 125I-labeled α bungarotoxin in normal and deafferented antennal lobes of Manduca sexta. *Proc. Natl. Acad. Sci. USA* **76**, 499-503. doi:10.1073/pnas.76.1.499

Homberg, U., Montague, R. A. and Hildebrand, J. G. (1988). Anatomy of antenno-cerebral pathways in the brain of the sphinx moth Manduca sexta. *Cell Tissue Res.* **254**, 255-281. doi:10.1007/BF00225800

Hösl, M. (1990). Pheromone-sensitive neurons in the deutocerebrum of Periplaneta americana: receptive fields on the antenna. *J. Comp. Physiol. A* **167**, 321-327. doi:10.1007/BF00192567

Husch, A., Paehler, M., Fusca, D., Paeger, L. and Kloppenburg, P. (2009). Calcium current diversity in physiologically different local interneuron types of the antennal lobe. *J. Neurosci.* **29**, 716-726. doi:10.1523/JNEUROSCI.3677-08.2009

Ito, K., Shinomiya, K., Ito, M., Armstrong, J. D., Boyan, G., Hartenstein, V., Harzsch, S., Heisenberg, M., Homberg, U., Jenett, A. et al. (2014). A systematic nomenclature for the insect brain. *Neuron* **81**, 755-765. doi:10.1016/j.neuron.2013.12.017

Kay, L. M. and Stopfer, M. (2006). Information processing in the olfactory systems of insects and vertebrates. *Semin. Cell Dev. Biol.* **17**, 433-442. doi:10.1016/j.semcdb.2006.04.012

Kristoffersen, L., Hansson, B. S., Anderbrant, O. and Larsson, M. C. (2008). Aglomerular hemipteran antennal lobes - basic neuroanatomy of a small nose. *Chem. Senses* **33**, 771-778. doi:10.1093/chemse/bjn044

Kuwahara, S. and Mori, K. (1990). Synthesis of (-)-periplanone-B a sex pheromone component of the American cockroach (periplaneta americana). *Tetrahedron* **46**, 8075-8082. doi:10.1016/S0040-4020(01)81464-2

Laissue, P. P., Reiter, C., Hiesinger, P. R., Halter, S., Fischbach, K. F. and Stocker, R. F. (1999). Three-dimensional reconstruction of the antennal lobe in Drosophila melanogaster. *J. Comp. Neurol.* **405**, 543-552. doi:10.1002/(SICI)1096-9861(19990322)405:4<543::AID-CNE7>3.0.CO;2-A

Lemon, W. and Getz, W. (1997). Temporal resolution of general odor pulses by olfactory sensory neurons in American cockroaches. *J. Exp. Biol.* **200**, 1809-1819.

Lockey, J. K. and Willis, M. A. (2015). One antenna, two antennae, big antennae, small: total antennae length, not bilateral symmetry, predicts odor-tracking performance in the American cockroach Periplaneta americana. *J. Exp. Biol.* **218**, 2156-2165. doi:10.1242/jeb.117721

Malun, D., Waldow, U., Kraus, D. and Boeckh, J. (1993). Connections between the deutocerebrum and the protocerebrum, and neuroanatomy of several classes of deutocerebral projection neurons in the brain of male Periplaneta americana. *J. Comp. Neurol.* **329**, 143-162. doi:10.1002/cne.903290202

Matsumoto, C. S., Matsumoto, Y., Watanabe, H., Nishino, H. and Mizunami, M. (2012). Context-dependent olfactory learning monitored by activities of salivary neurons in cockroaches. *Neurobiol. Learn. Mem.* **97**, 30-36. doi:10.1016/j.nlm.2011.08.010

Meijerink, J., Carlsson, M. A. and Hansson, B. S. (2003). Spatial representation of odorant structure in the moth antennal lobe: a study of structure-response relationships at low doses. *J. Comp. Neurol.* **467**, 11-21. doi:10.1002/cne.10914

Moreaux, L. and Laurent, G. (2007). Estimating firing rates from calcium signals in locust projection neurons in vivo. *Front. Neural Circuits* **1**, 2. doi:10.3389/neuro.04.002.2007

Nishino, H. and Mizunami, M. (2007). Sensilla position on antennae influences afferent terminal location in glomeruli. *Neuroreport* **18**, 1765-1769. doi:10.1097/WNR.0b013e3282f16d71

Nishino, H., Iwasaki, M., Paoli, M., Kamimura, I., Yoritsune, A. and Mizunami, M. (2018). Spatial receptive fields for odor localization. *Curr. Biol.* **28**, 600-608.e3. doi:10.1016/j.cub.2017.12.055

Nowotny, T., Stierle, J. S., Galizia, C. G. and Szyszka, P. (2013). Data-driven honeybee antennal lobe model suggests how stimulus-onset asynchrony can aid odour segregation. *Brain Res.* **1536**, 119-134. doi:10.1016/j.brainres.2013.05.038

Paoli, M., Andrione, M. and Haase, A. (2017). Imaging techniques in insects. In *Lateralized Brain Functions: Methods in Human and Non-Human Species* (ed. L. J. Rogers and G. Vallortigara), pp. 471-519. New York, NY: Springer New York.

Raiser, G., Galizia, C. G. and Szyszka, P. (2017). A high-bandwidth dual-channel olfactory stimulator for studying temporal sensitivity of olfactory processing. *Chem. Senses* **42**, 141-151. doi:10.1093/chemse/bjw114

Rybak, J., Kuß, A., Lamecker, H., Zachow, S., Hege, H.-C., Lienhard, M., Singer, J., Neubert, K. and Menzel, R. (2010). The digital bee brain: integrating and managing neurons in a common 3D reference system. *Front. Syst. Neurosci.* **4**, 30. doi:10.3389/fnsys.2010.00030

Sachse, S. and Galizia, C. G. (2002). Role of inhibition for temporal and spatial odor representation in olfactory output neurons: a calcium imaging study. *J. Neurophysiol.* **87**, 1106-1117. doi:10.1152/jn.00325.2001

Sachse, S., Rappert, A. and Galizia, C. G. (1999). The spatial representation of chemical structures in the antennal lobe of honeybees: Steps towards the olfactory code. *Eur. J. Neurosci.* **11**, 3970-3982. doi:10.1046/j.1460-9568.1999.00826.x

Sakura, M. and Mizunami, M. (2001). Olfactory learning and memory in the cockroach Periplaneta americana. *Zool. Sci.* **18**, 21-28. doi:10.2108/zsj.18.21

Sakura, M., Okada, R. and Mizunami, A. M. (2002). Olfactory discrimination of structurally similar alcohols by cockroaches. *J. Comp. Physiol. A Sens. Neural Behav. Physiol.* **188**, 787-797. doi:10.1007/s00359-002-0366-y

Salecker, I. and Boeckh, J. (1996). Influence of receptor axons on the formation of olfactory glomeruli in a hemimetabolous insect, the cockroachPeriplaneta americana. *J. Comp. Neurol.* **370**, 262-279. doi:10.1002/(SICI)1096-9861(19960624)370:2<262::AID-CNE9>3.0.CO;2-0

Sass, H. (1983). Production, release and effectiveness of two female sex pheromone components of Periplaneta americana. *J. Comp. Physiol. A* **152**, 309-317. doi:10.1007/BF00606237

Schafer, R. and Sanchez, T. V. (1973). Antennal sensory system of the cockroach, Periplaneta americana: Postembryonic development and morphology of the sense organs. *J. Comp. Neurol.* **149**, 335-353. doi:10.1002/cne.901490304

Schaller, D. (1978). Antennal sensory system of Periplaneta americana L. *Cell Tissue Res.* **191**, 121-139. doi:10.1007/BF00223221

Silbering, A. F., Okada, R., Ito, K. and Galizia, C. G. (2008). Olfactory information processing in the Drosophila antennal lobe: anything goes? *J. Neurosci.* **28**, 13075-13087. doi:10.1523/JNEUROSCI.2973-08.2008

Stensmyr, M. C., Dweck, H. K. M., Farhan, A., Ibba, I., Strutz, A., Mukunda, L., Linz, J., Grabe, V., Steck, K., Lavista-Llanos, S. et al. (2012). A conserved dedicated olfactory circuit for detecting harmful microbes in drosophila. *Cell* **151**, 1345-1357. doi:10.1016/j.cell.2012.09.046

Stierle, J. S., Galizia, C. G. and Szyszka, P. (2013). Millisecond stimulus onset-asynchrony enhances information about components in an odor mixture. *J. Neurosci.* **33**, 6060-6069. doi:10.1523/JNEUROSCI.5838-12.2013

Stocker, R. F., Heimbeck, G., Gendre, N. and de Belle, J. S. (1997). Neuroblast ablation in Drosophila P[GAL4] lines reveals origins of olfactory interneurons. *J. Neurobiol.* **32**, 443-456. doi:10.1002/(SICI)1097-4695(199705)32:5<443::AID-NEU1>3.0.CO;2-5

Strausfeld, N. J. and Li, Y. (1999). Organization of olfactory and multimodal afferent neurons supplying the calyx and pedunculus of the cockroach mushroom bodies. *J. Comp. Neurol.* **409**, 603-625. doi:10.1002/(SICI)1096-9861(19990712)409:4<603::AID-CNE7>3.0.CO;2-P

Szyszka, P., Gerkin, R. C., Galizia, C. G. and Smith, B. H. (2014). High-speed odor transduction and pulse tracking by insect olfactory receptor neurons. *Proc. Natl. Acad. Sci. USA* **111**, 16925-16930. doi:10.1073/pnas.1412051111

Tabuchi, M., Sakurai, T., Mitsuno, H., Namiki, S., Minegishi, R., Shiotsuki, T., Uchino, K., Sezutsu, H., Tamura, T., Haupt, S. S. et al. (2013). Pheromone responsiveness threshold depends on temporal integration by antennal lobe projection neurons. *Proc. Natl. Acad. Sci. USA* **110**, 15455-15460. doi:10.1073/pnas.1313707110

Takasaki, T., Namiki, S. and Kanzaki, R. (2012). Use of bilateral information to determine the walking direction during orientation to a pheromone source in the silkmoth Bombyx mori. *J. Comp. Physiol. A* **198**, 295-307. doi:10.1007/s00359-011-0708-8

Uchida, N., Takahashi, Y. K., Tanifuji, M. and Mori, K. (2000). Odor maps in the mammalian olfactory bulb: Domain organization and odorant structural features. *Nat. Neurosci.* **3**, 1035-1043. doi:10.1038/79857

Watanabe, H., Nishino, H., Nishikawa, M., Mizunami, M. and Yokohari, F. (2010). Complete mapping of glomeruli based on sensory nerve branching pattern in the primary olfactory center of the cockroach Periplaneta americana. *J. Comp. Neurol.* **518**, 3907-3930. doi:10.1002/cne.22452

Watanabe, H., Haupt, S. S., Nishino, H., Nishikawa, M. and Yokohari, F. (2012). Sensillum-specific, topographic projection patterns of olfactory receptor neurons in the antennal lobe of the cockroach Periplaneta americana. *J. Comp. Neurol.* **520**, 1687-1701. doi:10.1002/cne.23007

Watanabe, H., Nishino, H., Mizunami, M. and Yokohari, F. (2017). Two parallel olfactory pathways for processing general odors in a cockroach. *Front. Neural Circuits* **11**, 1-20. doi:10.3389/fncir.2017.00032

Watanabe, H., Koike, Y., Tateishi, K., Domae, M., Nishino, H. and Yokohari, F. (2018). Two types of sensory proliferation patterns underlie the formation of spatially tuned olfactory receptive fields in the cockroach *Periplaneta americana*. *J. Comp. Neurol.* **526**, 2683-2705. doi:10.1002/cne.24524

Zube, C., Kleineidam, C. J., Kirschner, S., Neef, J. and Rössler, W. (2008). Organization of the olfactory pathway and odor processing in the antennal lobe of the ant Camponotus floridanus. *J. Comp. Neurol.* **506**, 425-441. doi:10.1002/cne.21548

Supplementary Information

Supplementary Figure

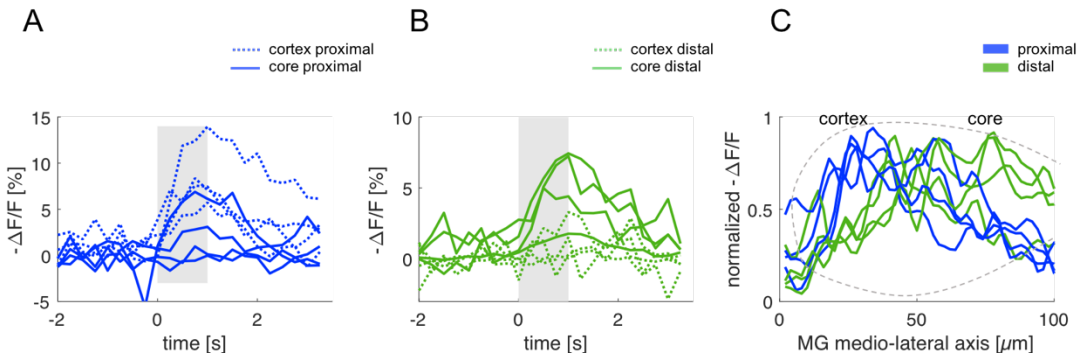

Figure S1. Antennotopic odour response in the macroglomerulus. Individual traces from four animals showing evoked responses in the MG core (continuous line) and cortex (dotted line) to a proximal (**A**) and a distal (**B**) stimulation. (**C**) Individual traces showing the evoked responses along the longitudinal MG axis for proximal and distal stimulation, where position 0 µm corresponds to the most lateral side and position 100 µm to the most medial side of the MG.

Supplementary Table

Table S1. Mean, s.e.m., and number of latency measurements presented in **Fig. 5C**.

ODORANT	DILUTION	POSITION [mm]	mean [ms]	s.e.m. [ms]	*n*
butanol	1:1	6	45,5	5,7	11
butanol	1:1	12	57,3	4,5	9
butanol	1:1	18	86,0	10,1	6
butanol	1:1	24	103,3	28,0	3
butanol	1:10	6	62,4	5,5	10
butanol	1:10	12	81,9	7,4	8
butanol	1:10	18	105,4	19,4	5
butanol	1:10	24	48,8	4,9	2
linalool	1:1	6	38,3	5,1	11
linalool	1:1	12	36,6	3,9	10
linalool	1:1	18	106,1	9,4	5
linalool	1:1	24	110,1	0,0	1
linalool	1:10	6	50,9	4,9	11
linalool	1:10	12	63,2	4,2	10
linalool	1:10	18	96,4	9,3	6
linalool	1:10	24	102,3	0,0	1
octanol	1:1	6	41,3	4,4	13
octanol	1:1	12	41,8	4,2	12
octanol	1:1	18	62,7	5,3	10
octanol	1:1	24	110,8	14,3	5
octanol	1:10	6	47,7	4,6	13
octanol	1:10	12	52,0	5,6	11
octanol	1:10	18	71,0	6,9	10
octanol	1:10	24	94,0	15,1	5
peppermint oil	1:1	6	25,1	4,2	14
peppermint oil	1:1	12	26,7	4,2	13
peppermint oil	1:1	18	56,5	5,7	11
peppermint oil	1:1	24	79,8	7,0	6
peppermint oil	1:10	6	38,5	4,4	14
peppermint oil	1:10	12	39,0	4,6	13
peppermint oil	1:10	18	64,0	5,6	10
peppermint oil	1:10	24	81,0	10,4	6

Supplementary Movies

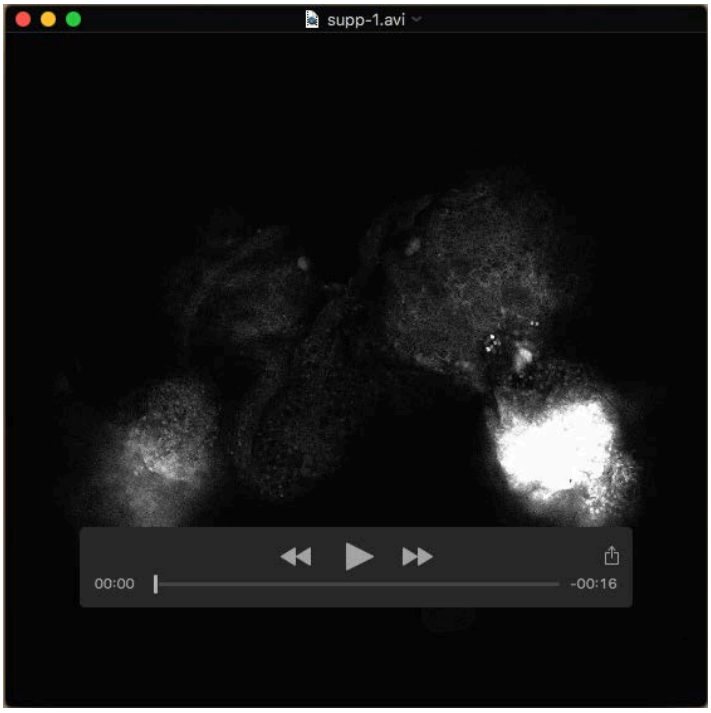

Movie 1. Bilateral antennal lobe dye injection reveals projection neurons tracts. Morphological z-stack of confocal images. Image size: 1190 × 1190 µm; z-interval between consecutive frames: 2 µm.

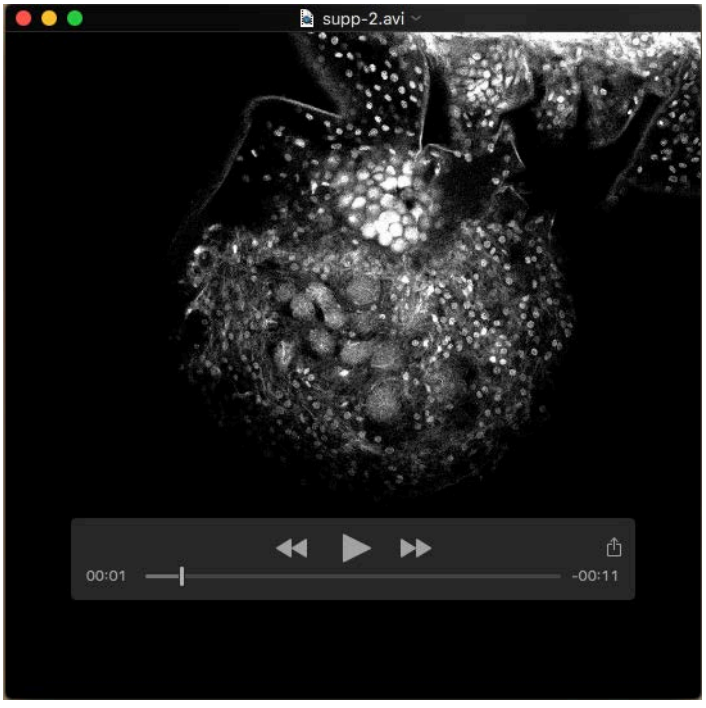

Movie 2. Z-stack of antennal lobe uniglomerular projection neurons labelling. PNs were stained by injecting a dye chrystal into the axonal tract. Image size: 643 × 643 µm; z-interval between consecutive frames: 3 µm.

Journal of Experimental Biology • Supplementary information

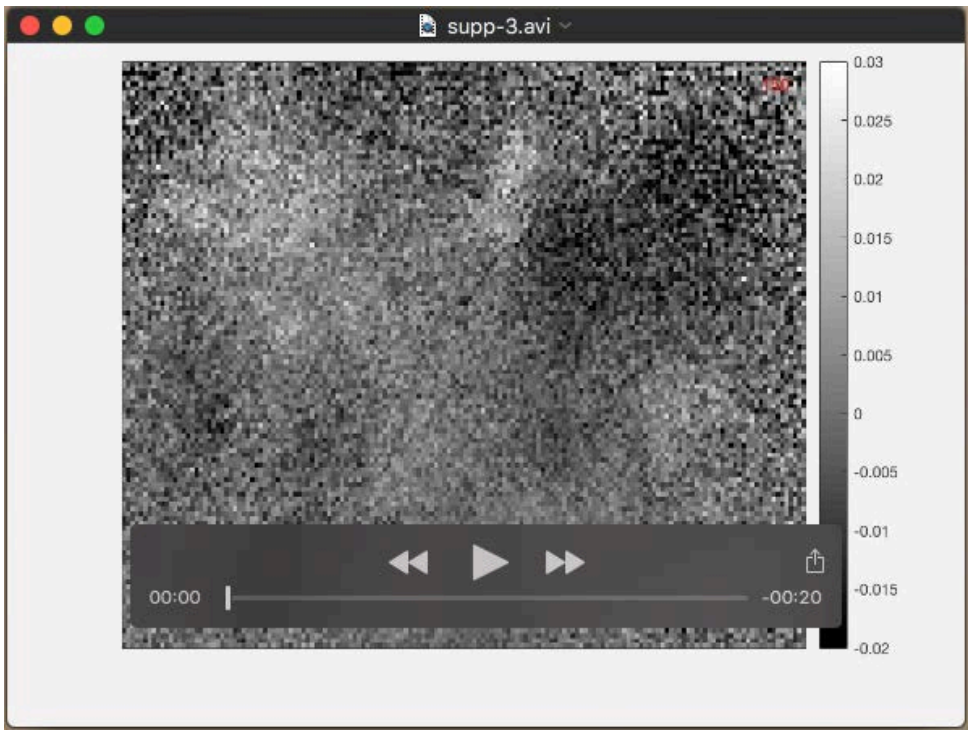

Movie 3. Antennal lobe spontaneous and stimulus-evoked activity. The video shows 20 s of calcium imaging in the projection neurons of the antennal lobe. While intense activity can be observed during stimulation (green rectangle), ongoing activity can be observed also before and after stimulation. Video was acquired at 25 Hz but presented at 12.5 Hz (every second section was omitted for reduce file size); stimulus (1-octanol 10^{-2}) was delivered two times for 0.1 s, at $t = 4$ s and $t = 14$ s. Colormap of raw data presented as $\Delta R_{340/380}$. No filtering or post-processing was applied to this video. Scale bar, 100 µm.